UCLouvain
Faculty of Science
Department of Physics
Earth and Life Institute

MODELLING RESILIENCE OF VEGETATION PATTERNS IN SEMI-ARID REGIONS FOR CHANGING PRECIPITATION CONDITIONS

DOCTORAL DISSERTATION PRESENTED BY

LILIAN VANDERVEKEN

IN PARTIAL FULFILLMENT OF THE REQUIREMENTS FOR THE DEGREE OF
DOCTOR IN SCIENCES OF THE UCLOUVAIN

THESIS COMMITTEE:

Michel Crucifix (Supervisor)	UCLouvain, Belgium
Max Rietkerk	Utrecht University, Netherlands
Robbin Bastiaansen	Utrecht University, Netherlands
Valentin Couvreur	UCLouvain, Belgium
Qiuzhen Yin	UCLouvain, Belgium

LOUVAIN-LA-NEUVE
MARCH 2025

Cette thèse a été un travail au long cours qui n'aurait pas été possbile sans l'aide et le soutien de nombreuses personnes que je voudrais remercier ici.

La première personne sans qui ce travail n'aurait jamais vu le jour est Michel Crucifix. Merci à toi Michel pour toutes ces années. J'ai compté que ca fait maintenant depuis presque dix ans que j'ai la chance de travailler avec toi. J'ai appris énormément à ton contact que ce soit scientifiquement ou dans d'autres domaines. J'apprécie beaucoup ta vision de la science et elle m'a beaucoup influencé tout au long de ces années de thèse. I also would like to thank the members of my jury Robbin Bastiaansen, Max Rietkerk and Valentin Couvreur for the discussions and comments that improved the quality of the thesis. Thank you also to Qiuzhen Yin for her participation as president of the jury. Merci à toute l'équipe de Michel pour les journal clubs inspirant. Merci à Livia, Dominique et Alice pour leur travail qui facilite grandement le nôtre. Merci à Marina avec qui j'ai eu la chance de partager mon bureau pendant la majorité de cette thèse. Nos discussions scientifiques m'ont sorti de l'ornière à de multiples reprises.

J'ai eu la chance durant cette thèse de m'impliquer et de présider dans deux association de chercheurs excpetionnelles; les YoungMinds UCLouvain et l'ACELI. Je tiens à remercier tous les membres de ces organisations avec lesquels j'ai eu l'occasion de collaborer et plus particulièrement Manon Ferdinand et Manon Nuytten, mes deux coprésidentes de l'ACELI.

Merci à tous les étudiants que j'ai eu la chance d'avoir dans mes classes et tous mes collègues assistants de l'école de physique.

Merci à tous les collègues (les actuels comme les anciens) du Mercator pour les discussions à la cafet ou autour des multiples bières. Votre soutien a été essentiel pour moi.

Je tiens aussi à remercier tous les amis de l'impros et d'ailleurs pour leur encouragement et soutien jusqu'au bout!

Merci enfin à mes parents et mon frère, pour leur support moral et relectures attentives de ce manuscript.

Et finalement merci à Cécile pour tout.

Summary

Semi-arid regions, like the Sahel, face significant challenges due to climate change. In these areas, vegetation forms spatial patterns to cope with water scarcity. Understanding the resilience of these patterns is crucial for predicting ecosystem responses to changing environmental conditions. This thesis investigates vegetation patterns in semi-arid ecosystems using the Rietkerk model, a system of partial differential equations. We focus on bifurcations, rate-induced tipping (R-tipping), and the effects of stochastic precipitation.

An in-depth bifurcation analysis of the Rietkerk model reveals stable patterned states even under low rainfall, where no vegetation persists in a homogeneous system. We identify and classify stable and unstable equilibria. We also discover "mixed states," novel unstable equilibria that slow down transitions between stable patterns and offer insights into tipping points in spatial systems.

To assess resilience, we examine the system's response to perturbations and link this response to internal timescales. The spatio-temporal structure of perturbations is crucial for resilience. The co-existence of multiple equilibria and unstable states enhances resilience by offering stable configurations under fluctuating conditions.

Finally, incorporating intermittent precipitation dynamics shows that the effects on vegetation depend on rainfall intermittency and water uptake. This research advances our understanding of vegetation pattern dynamics, offering a framework to assess ecosystem resilience in water-limited environments.

Contents

Contents **v**

1 Introduction **1**
1.1 Sahel in a changing world 1
1.2 Vegetation patterns and its modelling 3
1.3 Stability and resilience of vegetation patterns 6
1.4 Objectives and outlines of the thesis 9

2 Existence and influence of mixed states in a model of vegetation patterns **11**
2.1 Introduction 12
2.2 Bifurcation diagram and stability 14
2.3 Numerical simulations of trajectories 25
2.4 Discussion 27
2.5 Conclusions 29

3 Rate-induced transitions and noise-driven resilience in vegetation pattern dynamics **31**
3.1 Introduction 32
3.2 Model description 33
3.3 Effect of rainfall perturbation on vegetation dynamics: identifying critical timescales 34
3.4 Effect of Spatially and Temporally Structured Noise on Vegetation Pattern Resilience 38
3.5 Conclusions 42

4 Intermittent rainfall and vegetation patterns **45**
4.1 Introduction 46
4.2 Intermittent dynamical system as a model for precipitation. 48

4.3 Effect of intermittent rainfall on vegetation patterns 52
4.4 Conclusions 55

5 Conclusions and perspectives **57**
5.1 What are the possible intermediate states existing between a full vegetated state and bare soil and what is their influence on the dynamics? 57
5.2 How does the temporal and spatial structure of the perturbation affect the resilience of vegetation? 58
5.3 What is the impact of intermittent rainfall on vegetation resilience? 59
5.4 General conclusions 60
5.5 Scope, Limitations, and Future Perspectives 61

A Supplement to Chapter 2 **65**
A.1 Numerical method 65
A.2 Random initial conditions with a fixed rainfall 66
A.3 Identification of zero modes along branches 68

B Supplement to Chapter 3 **69**
B.1 Structured noise 69

C List of publications related to the thesis **73**

References **75**

1

Introduction

1.1 Sahel in a changing world

The Sahel is a semi-arid region in Africa, spanning several countries (Fig. 1.1) south of the Sahara Desert (Sinclair and Fryxell [1985], Govaerts and Lattanzio [2007]). Characterized by a single rainy season from June to September, the region experiences high rainfall variability [Buis et al., 2009]. Traditionally, the Sahel sustained migratory pastoralists and wild ungulate populations, but this balance was disrupted in the mid-20th century by increased settlement near wells, and agricultural expansion [Sinclair and Fryxell, 1985].

This region has been through multiple changes on a geological time scale. It is believed that those regions have undergone a transformation at the end of the African Humid Period, around 4.98 to 5.5 ka ago (Claussen et al. [1999]). Evidence from sediment records, such as increased dust deposition in the Atlantic, suggests

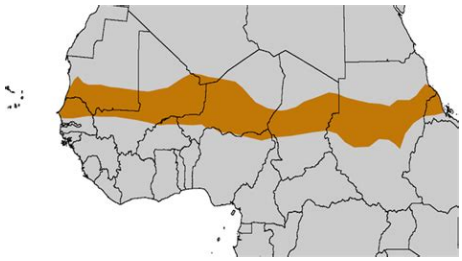


Figure 1.1: *Spatial extension of the Sahel (in orange) (from https://en.wikipedia.org/wiki/Sahelian_empires*

that this transition from a vegetated to arid landscape occurred swiftly [DeMenocal et al., 2000]. Researchers suggest that changes in orbital parameters reduced the temperature gradient between the ocean and the continent during summer, weakening the monsoon. This caused less precipitation on the land, which in turn decreased the vegetation cover. The decrease in vegetation cover causes an increase in surface albedo, which further weakens the monsoon through a feedback loop. This feedback, first proposed by Charney [1975], explains the persistence of desert conditions. Another positive feedback between precipitation and vegetation, suggested by Brovkin et al. [1998] and further explored by Scheffer et al. [2005], involves water recycling processes. The recycling feedback refers to the process by which water evaporates, condenses, and precipitates repeatedly within a specific region. Water that evaporates from surfaces like soil, vegetation, and water bodies returns as precipitation within the same area, creating a regional water recycling loop. This enhanced precipitation leads to an increase of vegetation cover and so an increased evapotranspiration. This feedback can be particularly significant in sustaining ecosystems, especially in semi-arid and tropical regions where local evapotranspiration contributes substantially to regional rainfall [Scheffer et al., 2005]. Both feedbacks operate on a climatic scale. Recently, Hopcroft and Valdes [2021] simulated a greener Sahara using an Earth System Model that incorporated enhanced parametrization of convective rainfall and semi-arid vegetation representation. However, their model did not reproduce a sharp transition for the eastern Sahel but rather a gradual change also observed in vegetation taxa data [Kröpelin et al., 2008].

In more recent history, multiple factors have contributed to environmental degradation in the Sahel. In addition to severe droughts observed mainly in the 70 and 80s that led to famines and impacted the environment, human activities such as population growth, overgrazing, and extensive agriculture also contributed to soil degradation and desertification (Bernus et al. [1993], Schlesinger et al. [1990]). The region's vulnerability is heightened by its dependence on volatile rainfall and the erosion of traditional adaptive practices such as migratory pastoralist [Walther and Retaillé, 2021]. With climate change expected to alter rainfall patterns (Intergovernmental Panel on Climate Change (IPCC) [2023], Chagnaud et al. [2023], Herman et al. [2023]), the Sahelian ecosystem faces additional challenges.

The vulnerability of the Sahelian ecosystem, combined with past transitions between vegetated and desert states (whether rapid or gradual), highlights the need to better understand vegetation resilience in semi-arid regions. A key feature of vegetation in these areas is its tendency toward self-organization that we will develop in the following chapters. In this thesis, we assess the resilience of vegetation patterns in semi-arid regions using a simplified model approach.

1.2 Vegetation patterns and its modelling

In semi-arid regions, vegetation organizes itself in patterns that are visible from the sky (Fig. 1.2). The first reported observation of such vegetation patterns by Macfadyen (Macfadyen [1950b], Macfadyen [1950a]) in British Somaliland was done from a plane. They appeared as bands perpendicular to the slope. Since then, vegetation patterns were observed in various places in the world (Valentin et al. [1999] , Rietkerk et al. [2004] Gandhi et al. [2019]) including African Sahel (Mueller [2013], Deblauwe et al. [2012], Bastiaansen et al. [2018]), Somalia (Hemming [1965], Gowda et al. [2018]), Australia (Dunkerley and Brown [2002], Moreno-De Las Heras et al. [2012]), Israel (Sheffer et al. [2013], Buis et al. [2009]), the US (Deblauwe et al. [2012], Penny et al. [2013] Pelletier et al. [2012]), and Northen Chile (Fernandez-Oto et al. [2019]). These observations revealed that banded vegetation on hill slope is not the only possible spatial configuration, and patterns formation is quite a common feature around the world, from arid ecosystems [Deblauwe et al., 2008] to wetlands [Rietkerk and van de Koppel, 2008a]. A surprising characteristic of those patterns is that they are not induced neither by heterogeneity in soil properties, nor by local topography [Borgogno et al., 2009]. In Deblauwe et al. [2011], the authors used satellite data from Sudan to confirm the dependence of vegetation patterns on both rainfall and slope. As previously identified, slope influences the alignment of vegetated bands, orienting them perpendicular to the incline. The study observed a transition from spotted to labyrinth-like and then dotted vegetation patterns as rainfall decreased from 1.6 to 1 $\mathrm{mm\,d^{-1}}$. The corresponding pattern wavelengths ranged from 40 to 150 meters, increasing as rainfall decreased.

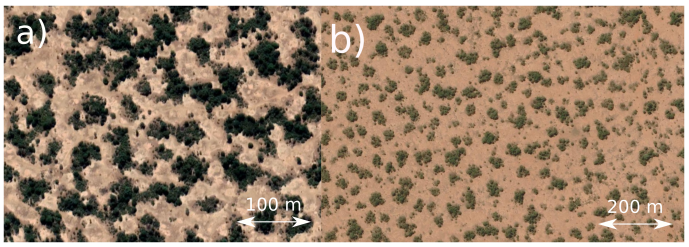


Figure 1.2: *Vertical satellite image of a) labyrinth (11° 8' N, 27° 57' E) and b) dots (11° 37' N, 27° 77' N) from Google Earth*

Vegetation patterns have interested researchers for multiple decades now. The first model to explain the self-organization of vegetation on hill slope was by Thiery et al. [1995]. The model is based on a cellular automata formalism [Conway, 1976]. Cellular automata are mathematical models composed of a grid of cells,

where each cell has a state that evolves over discrete time steps according to a set of rules. In the Thiery et al. [1995] model, two hypotheses were used which reflect competition and synergy: new vegetation appearance is positively affected by lateral and down-slope plants and negatively affected by plants up-slope. This formalism leads to a whole branch of vegetation patterns model that are still used today [Kéfi et al., 2007]. Two years later, Lefever and Lejeune [1997] proposed an other formalism based on integro-differential equations. In their model the patterns come from a mechanism of short-range activation, due to cooperation between plants of the same species, and long-range inhibition, due to competition among plants. This concept of short-range activation and long-range inhibition originated from the work of Turing [1952] on morphogenesis. In Lefever model, it is only the interaction of the plants with themselves that creates the patterns. Much later, Klausmeier [1999a] proposed a reaction-advection-diffusion model that adds water to the mix to explain the formation of vegetation bands on hill slope. Two quantities were modelled: the biomass and the soil water. The mechanism proposed to explain the self-organization is the following. In a desertic environment, water infiltration is lower on bare soil compared to a vegetated one, due to the system of roots. The increased production of biomass due to the infiltrated water in the soil creates a positive feedback. On a hill slope, the water coming from run-off up-slope on a bare ground goes in the soil on top of a band of vegetation due to the increased infiltration. This new water in the soil creates more vegetation and so creates an upward movement of the band. This model was extended later by the addition of a diffusion term for water that allowed creation of patterns on flat ground [Van Der Stelt et al., 2013]. HilleRisLambers et al. [2001] proposed a model for flat terrain that modelled more explicitly the water infiltration positive feedback, by taking into account the surface water and the soil water. This three-variables spatially explicit model of partial differential equations does not need any slope nor prexisting spatial heterogeneity to develop patterns. Rietkerk et al. [2002a] showed that this model is sufficient to explain all different vegetations observed in semi-arid ecosystem including dots (Fig. 1.2.b) , labyrinths (Fig. 1.2.a) and gaps. Crucially, the model suggests that patterns allow to increase the range on precipitation under which vegetation can maintain itself. Next, Gilad et al. [2004] added a root augmentation feedback (Zelnik et al. [2013], [Meron, 2015]). When upper-soil biomass increases, the lateral root extends more, so that plants can capture soil water from further away from their position.

The four models (Lefever and Lejeune [1997], Klausmeier [1999a], HilleRisLambers et al. [2001] and Gilad et al. [2004]) share the same mechanism of short-range facilitation and long-range competition. Due to this main characteristic, they are called scale-dependent models. Many vegetation patterns can be simulated with those four models, but they all share the same mechanism of patterns formation.

Besides the cellular automata and scale-depend models, there are other families of models that create patterns. For example, D'Odorico et al. [2006] showed how patterns could be obtained from a repeated random switch between two deterministic processes corresponding to stressed and unstressed conditions. Lately, a new framework based on phase-separation physics has been proposed (Liu et al. [2016], Siteur et al. [2023]). This new conceptual framework involves the aggregation of an abiotic or biotic species into non-regular patches.

In this thesis, we will focus on scale-dependent models and more precisely on the model described in Rietkerk et al. [2002a]. This model features three (prognostic) variables: biomass (B) [g.m^{-2}], soil water (W) [mm] and surface water (O) [mm], all are functions of time and space. The evolution of those quantities are governed by three equations:

$$\begin{aligned}
\frac{\partial B}{\partial t} &= cg_{max}\frac{W\,B}{W+k_1} - dB + D_B\Delta B,\\
\frac{\partial W}{\partial t} &= \alpha O\frac{B+k_2w_0}{B+k_2} - g_{max}\frac{W\,B}{W+k_1} - r_wW + D_W\Delta W,\\
\frac{\partial O}{\partial t} &= R - \alpha O\frac{B+k_2w_0}{B+k_2} + D_O\Delta O,
\end{aligned} \tag{1.1}$$

where Δ is the Laplacian operator and R is the rainfall [mm.d^{-1}]. The rainfall is the external forcing of the system which we consider to be a spatially-independent function. The first term in the biomass equation represents water uptake by the plant. The parameters of the water uptake are k_1 the half-saturation constant of specific plant growth and water uptake, c the conversion of water uptake by plants to plant growth and g_{max} the maximum water uptake. The first term in the soil water equation is linked to the infiltration rate of water in the soil that is enhanced by the presence of biomass. α is the maximum infiltration rate, k_2 the saturation constant of water infiltration and w_0 the infiltration rate in the absence of plants. Soil water is lost through moving out of plant roots by drainage or evaporation. This effect is parametrised with r_w. The plant mortailty is modelled with a linear term with d the plant mortality rate. The value of this mortality rate was fixed at 0.25d^{-1} which could be considered as high depending the type of vegetation. The factors in front of the Laplacians (D_B, D_W and D_O) are the diffusion constants of the different quantities. In this thesis, we used the model with a flat ground so all the diffusion parameters are constant. All values of the different parameters are given in the table 1.1. The values of the parameters were chosen as in Rietkerk's original paper [Rietkerk et al., 2002a]. The diffusion constant for surface water (D_O) is significantly higher than those of biomass (D_B) and soil water (D_W). This difference, combined with the infiltration feedback, is key to explain pattern formation in semi-arid ecosystems. The short-range activation process involves an increase in soil water concentration beneath vegetation due to enhanced infiltration, which, in

c	Conversion of water uptake by plants to plant growth	$10\,\mathrm{g\,mm^{-1}\,m^{-2}}$
g_{max}	Maximum water uptake	$0.05\,\mathrm{mm\,g^{-1}\,m^2\,d^{-1}}$
k_1	Half-saturation constant of specific plant growth and water uptake	$5\,\mathrm{mm}$
D_B	Plant dispersal	$0.1\,\mathrm{m^2\,d^{-1}}$
α	Maximum infiltration rate	$0.2\,\mathrm{d^{-1}}$
k_2	Saturation constant of water infiltration	$5\,\mathrm{g\,m^{-2}}$
w_0	Water infiltration in the absence of plants	0.2
r_w	Soil water loss due to evaporation and drainage	$0.2\,\mathrm{d^{-1}}$
D_W	Diffusion coefficient for soil water	$0.1\,\mathrm{m^2\,d^{-1}}$
D_O	Diffusion coefficient for surface water	$100\,\mathrm{m^2\,d^{-1}}$
d	Plant mortality rate	$0.25\mathrm{d^{-1}}$

Table 1.1: *Parameters for Rietkerk model*

turn, promotes biomass growth. In contrast, the long-range inhibition process results from rapid surface water diffusion from bare soil areas to vegetated patches. This surface water depletion around vegetation patches reduces the water available for surrounding areas, thereby limiting vegetation spread and confining it to existing patches.

While this model reproduces well patterns with a width around a tens of meters as the one shown in Fig. 1.2, it also models the presence of a shallow layer of water above ground which is not realistic for arid regions. While this model includes a shallow layer of water above the ground, which may not be realistic for arid regions, it successfully reproduces patterns with widths on the order of tens of meters, as shown in Fig. 1.2.

1.3 Stability and resilience of vegetation patterns

How ecosystems adapt to a perturbation (human or climatic) is at the core of ecology. Before the 1970s, the resilience of an ecosystem was defined as the ability of a system to return to an equilibrium state after a temporary disturbance. The definition was inspired from mathematics and physics: The fastest the ecosystem returns to equilibrium, and the smallest is the amplitude of the fluctuation, the more stable it is. This definition of resilience is consistent with the concept of early warnings signals which flourished a few decades later (Dakos et al. [2008], Dakos et al. [2019], Boers [2021]). In climatology, early warning signals are indicators or patterns in climate data that suggest an approaching critical change or transition in a climate system. These signals are intended to help predict potential abrupt shifts or "tipping points" in the climate, where the system moves from one stable state to another. Holling [1973] described this form of resilience, based on the return time as "engineer resilience". He suggested to distinguish it from a more proper "ecological resilience". According to Holling, ecological resilience should

be defined as the ability of a system to maintain its function and is measured by its capacity to absorb changes in state variables. There are four key aspects of ecological resilience [Walker et al., 2004]:

- Latitude – the extent to which a system can change before losing stability.
- Resistance – the ease or difficulty of altering the system.
- Precariousness – the proximity of the system's current state to a critical threshold.
- Panarchy – the influence of cross-scale interactions, where dynamics at a given scale depend on processes occurring at both larger and smaller scales.

These aspects are well-defined in systems with two alternative states—one favorable and one unfavorable. We propose extending the concept of ecological resilience to include systems with multiple desirable states, such as different spatial configurations of vegetation.

To illustrate that idea, let us consider two Pseudo-Lyapunov potentials of a semi-arid environment, as sketched in Fig. 1.3. The function of vegetation in this context is maximized when there is more biomass. For both potentials the red dot represents a state with low vegetation so a non-desirable state. From an engineer stability point of view, the green dot situation on the panel (a) is more enviable than the blue dot because the well is deeper and the slope of the well potential is steeper so the system will take less time to return to its initial position. The blue dot (panel (b)) still has ecological resilience because the presence of other desirable states around it makes it able to maintain its function eventhougth it left the basin of attraction of its initial conditions. In vegetation patterns, vegetation has the possibility to organise itself in different ways. This multiplicity of equilibria increases then the ecological resilience. The system is more capable of maintaining its function (high vegetation cover in the blue dot situation) even if is is kicked out of its orignal basin of attraction by a perturbation.

The resilience of vegetation patterns was studied in many ways in the literature. Rietkerk et al. [2002b] showed that the addition of a spatial component increases the range of precipitation for which vegetation still exists in the form of patterns. Multiple states were found in the so-called Busse-Balloon, defined as the range of environmental parameters from which a stable pattern state exists, in the mathematical sense (Van Der Stelt et al. [2013], Doelman et al. [2012], Siteur et al. [2014b], Siero et al. [2015]). Multiple stable vegetation patterns were then identified in real ecosystems [Bastiaansen et al., 2018]. This multistability increases, in our extended definition, the ecological resilience of vegetation. Adding a spatial

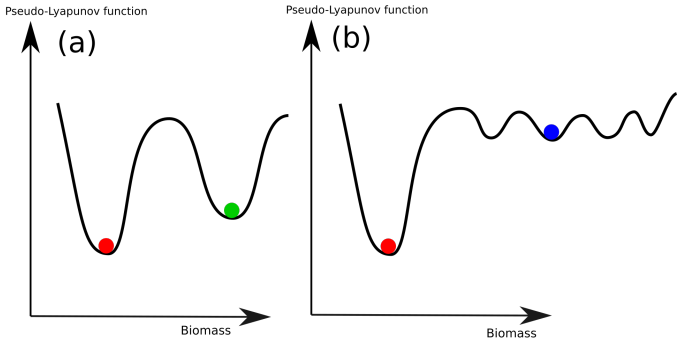


Figure 1.3: *Pseudo-Lyapunov function (or potential) to illustrate the notions of engineer resilience and ecological resilience. Local minima of this function are stable equilibira for the associated dynamical system.*

component when considering vegetation resilience also creates the possibility of front propagation. Multiple studies (Zelnik et al. [2017], Zelnik and Meron [2018] and Van De Leemput et al. [2015]) showed that, in the bistable range, an ecosystem can switch after a local disturbance — removing a small portion of vegetation — from a full vegetated state to a bare soil state through front propagation if the environmental parameter crosses a certain value, called the Maxwell point, even though both vegetated and bare soil state are stable. Zelnik et al. [2016] showed that if the system supports a specific class of stable patterns equilibria (hybrid state), a local disturbance can be absorbed by the system by switching to an other stable hybrid state.

Disturbances are generally characterized as one-dimensional (in space or time) in studies. However, Kéfi et al. [2019] points to the importance of the definition of perturbations when talking about resilience. More recently, Rietkerk et al. [2021] proposed that the existence of spatial patterns is an effective way to *evade* tipping points, and pointed out the necessity to study the resilience of an ecosystem taking into account the spatial components. Specifically, one must study the effects of the restricting spatial domain, and study both the local and non-local aspects of the perturbation, in time and in space. Throughout this thesis, we address the question of patterns resilience against different perturbations in an original way. The bifurcation diagram is our main tool. Previously, Zelnik et al. [2013] showed that the computation of a part of the bifurcation diagram helped to understand the resilience for a specific range of precipitation. We extend the study of multistability by identifying not only the stable, but also the unstable equilibria. The bifurcation diagram allows us to study both types of equlibiria, and we do so because we know

that both may play a role in the dynamics of the system (Hastings et al. [2018a], Morozov et al. [2020a], Feudel [2023])

1.4 Objectives and outlines of the thesis

In this thesis, we study the resilience of vegetation patterns by using Rietkerk model [Rietkerk et al., 2002b] and explore the effect of different perturbations. This objective will be tackled through three specific research questions:

- What are the possible intermediate states existing between a fully vegetated state and bare soil and what is their influence on the dynamics?
- How does the temporal and spatial structure of the perturbation affect the resilience of vegetation?
- What is the impact of intermittent rainfall on vegetation resilience?

Each chapter is devoted to one question. In the second chapter, we show the existence of previously unknown equilibria by a continuation method, and we discuss the effect of those equilibria on the dynamics. In the third chapter, we discuss how the nature of the perturbation affects the resilience and how it is possible to link the structure of the most destructive perturbations to time scales identified in the model. In the fourth chapter, we analyse the effect of precipitation intermittency. We model precipitation in semi-arid regions using an intermitent dynamical system [Pomeau and Manneville, 1980], and show that both the statistics of the intermittent forcing and the nature of the functional form of water uptake are critical to understand the response of the vegetation patterns to an intermittent forcing. Chapter 5 delivers the main conclusions and contributions of this thesis, along with the perspectives.

2

Existence and influence of mixed states in a model of vegetation patterns

This chapter is based on the following published paper:
Vanderveken, L., Martínez Montero, M. and Crucifix, M.: Existence and influence of mixed states in a model of vegetation patterns, *Nonlinear Processes in Geophysics*, **30(4)**, 585–599, https://doi.org/10.5194/npg-30-585-2023

Abstract

The Rietkerk vegetation model is a system of partial differential equations, which has been used to understand the formation and dynamics of spatial patterns in vegetation ecosystems, including desertification and biodiversity loss. Here, we provide an in-depth bifurcation analysis of the vegetation patterns produced by Rietkerk's model, based on a linear stability analysis of the homogeneous equilibrium of the system. Specifically, using a continuation method based on the Newton-Raphson algorithm, we obtain all the main heterogeneous equilibria for a given size of the domain. We confirm that inhomogeneous vegetated states can exist and be stable, even for a value of rainfall for which no vegetation exists in the non-spatialized system. In addition, we evidence the existence of a new type of equilibrium, which we called "mixed state", in which the equilibria are always unstable and take the form of a mix of two equilibria from the main branches. Although these equilibria are unstable, they influence the dynamics of the transitions between distinct stable states, by slowing down the evolution of the system when it passes close to it. Our approach proves to be a helpful way to assess the existence of tipping points in spatially extended systems and disentangle the fate of the system in the Busse balloon. Overall, our findings represent a significant step forward in

understanding the behaviour of the Rietkerk model and the broader dynamics of vegetation patterns.

2.1 Introduction

In semi-arid regions, vegetation tends to be spatially organized around patterns (Barbier et al. [2006], Deblauwe et al. [2008], Deblauwe et al. [2011], Deblauwe et al. [2012]). This phenomenon appears in various parts of the world where water is the limiting factor for plants' growth. Vegetation patterns can be modelled and explained with reaction-diffusion equations. Those types of equation exhibit the existence of a homogeneous stable equilibrium which is unstable to heterogeneous perturbation [Turing, 1952]. In general terms, heterogeneous equlibria result from the joint effects of a short-range activation mechanism and long-range inhibition. For vegetation on ferruginous soil in semi-arid regions, the short-range activation effect is related to the positive feedback of vegetation on soil water availability, as vegetation limits water loss by runoff by enhancing water infiltration [Meron, 2015].

The rapid diffusion of surface water, however, acts against vegetation growth on bare soil by limiting water availability. The contrast between slow soil water diffusion and fast surface water diffusion produces the spatial, heterogeneous patterns. The mechanisms are described and captured in the Rietkerk model [Rietkerk et al., 2002a]. This model features three (prognostic) variables: biomass (B) [g m^{-2}], soil water (W) [mm] and surface water (O) [mm], all are functions of time and space. The evolution of those quantities are governed by three equations:

$$\begin{aligned}
\frac{\partial B}{\partial t} &= cg_{max}\frac{W\,B}{W+k_1} - dB + D_B\Delta B,\\
\frac{\partial W}{\partial t} &= \alpha O\frac{B+k_2w_0}{B+k_2} - g_{max}\frac{W\,B}{W+k_1} - r_wW + D_W\Delta W,\\
\frac{\partial O}{\partial t} &= R - \alpha O\frac{B+k_2w_0}{B+k_2} + D_O\Delta O,
\end{aligned} \tag{2.1}$$

where Δ is the Laplacian operator and R is the rainfall [mm d^{-1}]. The rainfall is the external forcing of the system which we consider to be a spatially-independent function. The first term in the biomass equation represents water uptake by the plant. The first term in the soil water equation is linked to the infiltration rate of water in the soil that is enhanced by the presence of biomass. The factors in front of the Laplacians (ΔB, ΔW and ΔO)are the diffusion constants of the different quantities. The diffusion constant for surface water is considered to be much bigger than those of biomass and soil water. This contrast is essential for pattern creation. In the following, the values of the parameters are as in [Rietkerk et al., 2002a].

c	Conversion of water uptake by plants to plant growth	$10\,\mathrm{g\,mm^{-1}\,m^{-2}}$
g_{max}	Maximum water uptake	$0.05\,\mathrm{mm\,g^{-1}\,m^2\,d^{-1}}$
k_1	Half-saturation constant of specific plant growth and water uptake	$5\,\mathrm{mm}$
D_B	Plant dispersal	$0.1\,\mathrm{m^2\,d^{-1}}$
α	Maximum infiltration rate	$0.2\,\mathrm{d^{-1}}$
k_2	Saturation constant of water infiltration	$5\,\mathrm{g\,m^{-2}}$
w_0	Water infiltratio nin the absence of plants	0.2
r_w	Soil water loss due to evaporation and drainage	$0.2\,\mathrm{d^{-1}}$
D_W	Diffusion coefficient for soil water	$0.1\,\mathrm{m^2\,d^{-1}}$
D_O	Diffusion coefficient for surface water	$100\,\mathrm{m^2\,d^{-1}}$
d	Plant mortality rate	$0.25\mathrm{d^{-1}}$

Table 2.1: *Parameters for Rietkerk's model*

As explained above, the existence of reaction-diffusion processes enables stable equilibria in the form of patterns. Compared to a system without spatial dynamics, such pattern equilibria tend to broaden the range of rainfall compatible with the presence of vegetation.

The classical configuration for analysing such a system of equations uses periodic boundary conditions. A pattern is then defined as a spatially periodic equilibrium of the differential equations. Here, we will consider and analyse in depth a region of the parameter space called the Busse balloon [Busse, 1978]. This is the region with heterogeneous equilibria, that is, the parameter space admitting at least one stable, spatially periodic equilibrium.

The motivating scientific question comes from the following observation. In a system without spatial dynamics — thus without diffusion — a catastrophic transition occurs between sustained vegetation and bare soil when rainfall decreases below a critical point.

The transition point corresponds to a fold bifurcation, and can be qualified as a tipping point (Lenton et al. [2008]. Rietkerk et al. [2021]) suggested that spatial dynamics and the existence of the Busse ballon smooth the transition between fully fledged vegetation and bare soil. In their terms, the Busse Balloon 'evades' the tipping point. This result implies that spatial dynamics effectively lower the precipitation threshold above which vegetation can be sustained.

Siteur et al. [2014b] showed that a Busse balloon appears in the Klaussemeier vegetation model [Klausmeier, 1999a], where it occupies a region of the parameter space with lower rainfall than necessary to sustain a homogeneous vegetation. However, the nature of this transition through the Busse Balloon may be complex. For the non-spatial Rietkerk model, there is no such thing as a fold bifurcation. But we will see that adding a spatial component creates fold bifurcation.

The objective of the present study is, in the idealized context of a spatial domain of one dimension, to characterize the intermediate states that may emerge during the transition from full vegetation to bare soil, and to examine the dynamics that underlie potential transitions between these states.

Specifically, we provide an in-depth analysis of the Busse balloon, demonstrate the coexistence of multiple equilibria for a given rainfall intensity, and foresee the circumstances which may trigger transitions between these different equilibria. In that sense, we propose an extension of the work by Zelnik et al. [2013], who computed partially the bifurcation diagram for Rietkerk's model. We also develop the method for finding equilibrium branches and characterize their stability. Finally, we highlight the existence of another type of equilibrium different than the regular patterns. We call them mixed state because of their shape and show how they can have an influence on the dynamics of the system.

2.2 Bifurcation diagram and stability

In this section, we present a method to construct the bifurcation diagram for Rietkerk's model and determine the form of the different equilibrium branches as a function of rainfall.

Linear analysis and Turing zone

The classical approach is to consider as in Siero [2020], first, the static homogeneous equilibrium. To this end, we define the equilibrium $\bar{B} = B(x,t)$ with $\bar{B}$ a constant in time and space—likewise with the other variables—which satisfy the relationships:

$$0 = c g_{max} \frac{\bar{W}\,\bar{B}}{\bar{W} + k_1} - d\bar{B} \tag{2.2}$$

$$0 = \alpha O \frac{\bar{B} + k_2 w_0}{\bar{B} + k_2} - g_{max} \frac{\bar{W}\,\bar{B}}{\bar{W} + k_1} - r_w \bar{W} \tag{2.3}$$

$$0 = R - \alpha \bar{O} \frac{\bar{B} + k_2 w_0}{\bar{B} + k_2}. \tag{2.4}$$

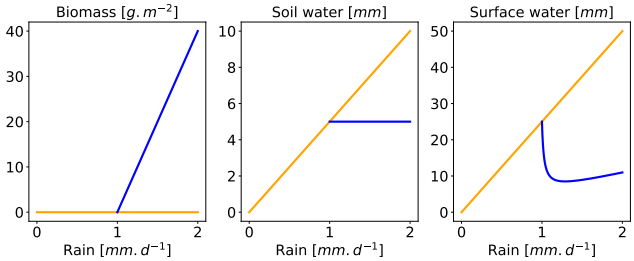


Figure 2.1: *Homogeneous equilibria of Rietkerk's model. From left to rigth are represented the biomass, the soil water and the surface water. Blue line is the equilibrum with vegetation, yellow is without.*

Two solutions exist depending on the value of R. One solution with vegetation is:

$$\bar{B} = c\left(\frac{R}{d} - \frac{k_1 r_w}{cg_{max} - d}\right), \tag{2.5}$$

$$\bar{W} = \frac{dk_1}{cg_{max} - d}, \tag{2.6}$$

$$\bar{O} = \frac{R((cg_{max} - d)(cR + dk_2) - cdk_1 r_w)}{\alpha((cg_{max} - d)(cR + dk_2 w_0) - cdk_1 r_w)}. \tag{2.7}$$

$$\tag{2.8}$$

Physical equilibria for positive parameters must be positive, and hence satisfy the relations $cg_{max} > d$ and $R > k_1 r_w d/(cg_{max} - d)$. The homogeneous equilibria without vegetation are, by definition, $\bar{B} = 0$, which implies

$$\bar{W}_0 = \frac{R}{r_w} \tag{2.9}$$

$$\bar{O}_0 = \frac{R}{w_0 \alpha}, \tag{2.10}$$

which are, again, valid for positive parameters. For the parameters chosen here, the homogeneous vegetated equilibrium exists for $R > 1$ and the non-vegetated equilibrium always exists[1]. Fig. 2.1 shows these equilibria as a function of rainfall R.

[1] The universal existence of the non-vegetated equilibrium does not imply its stability for all values of R.

We now consider the stability of these equilibria. Again, following standard practice we consider spatially periodic perturbations as follows:

$$B(x,t) = \bar{B} + \epsilon\delta B(x,t), \tag{2.11}$$
$$W(x,t) = \bar{W} + \epsilon\delta W(x,t), \tag{2.12}$$
$$O(x,t) = \bar{O} + \epsilon\delta O(x,t), \tag{2.13}$$

with

$$\delta B(x,t) = \delta B e^{\Omega t + i\kappa x}, \tag{2.14}$$
$$\delta W(x,t) = \delta W e^{\Omega t + i\kappa x}, \tag{2.15}$$
$$\delta O(x,t) = \delta O e^{\Omega t + i\kappa x}. \tag{2.16}$$

We now introduce the perturbation into the original equations, develop a Taylor expansion for small ϵ and get rid of the 0th order term by using the homogeneous equilibrium. The linearized equations obtained can be recast as an eigenvalue problem:

$$A = \begin{pmatrix} d - \frac{cg_{max}\bar{W}}{k_1+\bar{W}} + D_B\kappa^2 & -\frac{cg_{max}k_1\bar{B}}{(k_1+\bar{W})^2} & 0 \\ \frac{g_{max}\bar{W}}{k_1+\bar{W}} + \frac{k_2\alpha(w_0-1)\bar{O}}{(k_2+\bar{B})^2} & r_w + \frac{g_{max}k_1\bar{B}}{(k_1+\bar{W})^2} + D_W\kappa^2 & -\frac{\alpha(k_2w_0+\bar{B})}{k_2+\bar{B}} \\ -\frac{k_2\alpha(w_0-1)\bar{O}}{(k_2+\bar{B})^2} & 0 & \frac{\alpha(k_2w_0+\bar{B})}{k_2+\bar{B}} + D_O\kappa^2 \end{pmatrix} \begin{pmatrix} \delta B \\ \delta W \\ \delta O \end{pmatrix} = -\Omega \begin{pmatrix} \delta B \\ \delta W \\ \delta O \end{pmatrix} \tag{2.17}$$

Every pair of values (R,κ) defines a new eigenvalue problem. It corresponds to the linear dynamics obtained by perturbing a homogeneous equilibrium that exists at a particular value of R with wavenumber κ. We are interested in finding out whether there are values of (R,κ) for which there exists an exponentially growing solution, thus positive Ω. It is then said that the homogeneous equilibrium for a specific value of R is linearly unstable to perturbations of wavenumber κ. For the eigenvalue problem to have a non-trivial solution, the determinant $det(A+\Omega)$ must be 0. This leads to a cubic equation for Ω:

$$a_1(R,\kappa)\Omega^3 + a_2(R,\kappa)\Omega^2 + a_3(R,\kappa)\Omega + a_4(R,\kappa) = 0, \tag{2.18}$$

which we solve numerically on a physical domain defined by $\{R,\kappa\} \in \mathcal{R}$ with $R \geq 0$. This leads to three roots at each point in the domain, which we can refer to as $\Omega_1(R,\kappa)$, $\Omega_2(R,\kappa)$ and $\Omega_3(R,\kappa)$. Two of the roots, say $\Omega_{(2,3)}(R,\kappa)$, always have a real negative value, and hence correspond to exponentially decaying modes. One of the roots, $\Omega_1(R,\kappa)$, which is real in all the domain, has a positive real part in a region of the (R,κ) plane. The countour of this area is shown in Fig. 2.2 by the black line. This defines the *Turing zone*. Hence, for those values of (R,κ) with positive real part of Ω_1 (inside of the contour) the corresponding homogeneous equilibrium is linearly unstable to inhomogeneous perturbations of wavenumber κ.

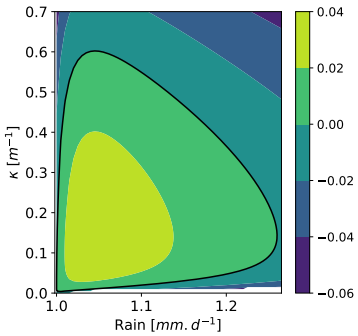


Figure 2.2: *Contour plot for $\Omega_1(R,\kappa)$. The thick black line is the contour $\Omega_1 = 0$ and the region inside that contour corresponds to the parameter region (R,κ) in which the homogeneous equilibria is linearly unstable against inhomogeneous perturbations, i.e., $\Omega > 0$.*

Zero modes correspond to marginally non-growing inhomogeneous solutions of the linearized equations and correspond to perturbations with $\Omega = 0$. Their existence usually signals the presence of an instability that can send the system towards an inhomogeneous time-invariant solution in the full nonlinear model. Specifically, Fig. 2.2 suggests the existence of two zero modes for any value of rainfall comprised between critical bounds 1.0mm d^{-1} and 1.25mm d^{-1}. Such zero modes can satisfy the boundary conditions for a (low) wavenumber that depends on R, and therefore require a domain large enough to develop. If the domain is so small that its fundamental mode is in the stable region ($\kappa \gtrsim 0.6$), it is always stable. In this section, we found zero modes along the homogeneous branch compatible with a specific domain. Those zero modes indicate the start of inhomogeneous branches of equilibria. In the following section we will rely on those zero modes to compute equilibria of the full nonlinear model.

2.2.1 Bifurcation diagram and continuation method

The analysis in the previous section showed that homogeneous vegetation is linearly unstable against spatially periodic perturbations in the rain range $1\text{mm d}^{-1} < R < 1.25\,\text{mm d}^{-1}$. This linear analysis suggested the existence of periodic inhomogeneous equilibria in the nonlinear system within that rainfall range. Now, our focus shifts towards explicitly computing these nonlinear equilibria. To achieve this, numerical methods are employed to solve the equations involved.

For the time being we assume a periodic domain with a finite size of $L = 100$ m. The choice of the size of the domain influences the number of zero modes exhibited on the homogeneous equilibrium branch. This choice, together with periodic boundary conditions, effectively discretizes the set of zero modes (Fig. 2.3).

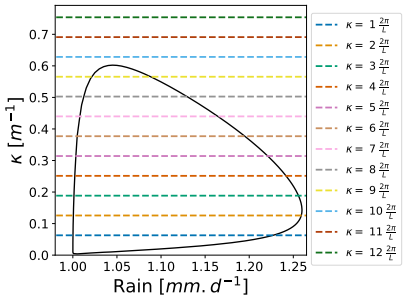


Figure 2.3: *Zero modes present in a domain of $L = 100\,m$. Horizontal lines correspond to harmonics that fit inside the periodic $L = 100$ domain. The intersection of the horizontal lines with the $\Omega_1 = 0$ contour provides the values of rain R at which new branches of equilibria might appear. Notice that each of the 9 horizontal lines that intersect the contour, intersect it twice, hence 18 zero modes.*

Indeed, setting $\kappa = n\frac{2\pi}{L}$, with n the wavenumber, we find two pairs (κ, R) corresponding to zero modes, with the range $\kappa = [0 : 0.6]$, corresponding to perturbing the homogeneous equilibrium $\bar{S}(R)$ with a perturbation $\delta S(x) = \delta S \cos(\kappa x)$.

For each pair of (κ, R) in the set of zero modes, we identify the corresponding homogeneous equilibrium $(\bar{S})$ and perturb it with the corresponding perturbation $\delta S \cos(\kappa x)$. The periodic boundary conditions are enforced by setting $\kappa = n\frac{2\pi}{L}$, with n the wavenumber. The perturbed homogeneous solution

$$B_0(x, R) = \bar{B} + \delta B cos(\kappa x), \tag{2.19}$$

$$W_0(x, R) = \bar{W} + \delta W cos(\kappa x), \tag{2.20}$$

$$O_0(x, R) = \bar{O} + \delta O cos(\kappa x), \tag{2.21}$$

is then taken as the first-guess input in a Newton-Raphson iteration used for finding the corresponding nonlinear inhomogeneous equilibrium.

At this point we need to discretize the spatial domain into N points. We used $N = 100$. Specifically, the discretized first guess reads

$$u_0(R) = [B_0(R), W_0(R), O_0(R)] \in \mathbb{R}^{3N}$$

and the algorithm

$$u_{i+1}(R) = u_i(R) - \epsilon J^{-1}(u_i(R)) f(u_i(R)), \tag{2.22}$$

converges towards the equilibrium $u_S(R)$ with $J(u_i(R))$ being the Jacobian matrix of the system and $f(u_i(R))$ being the right-hand side (as in Eq. (2.1)). The ϵ is fixed at a low value $(0,01)$ at the beginning of the method to insure that the algorithm does not send the system to another basin of attraction. The value of ϵ is

then increased (up to 1) when the algorithm is closer to the solution. The Laplacian operator is discretized with a periodic pseudospectral method (see Appendix 1. for more details). To allow the algorithm to converge towards equilibria where the jacobian matrix is close to non invertible, we added two tresholds to stop the algorithm. The first one is on the source term ($|max(f(u_i(R)))|$) and the second one on the update term ($|max(\epsilon J^{-1}(u_i(R))f(u_i(R)))|$). If both those terms are below their specified treshold ($[\sim 10^{-6}, \sim 10^{-10}]$), the algorithm stops. This equilibrium, $u_S(R)$, is then used as the first guess to solve for the equilibrium with rainfall $R + \delta R$,

$$u_0(R + \delta R) = u_S(R) + \delta u, \tag{2.23}$$

with $|\delta u| \ll 1$. This iterative procedure leads to the construction of the full branch of equilibria.

A new code has been developed to implement this continuation method. This code is available online in the repository mentioned in the Appendix 1.

Each branch obtained by the above technique is denoted by n between 1 and 9, with n the wavenumber associated with the perturbation. The periodic boundary conditions, together with a finite domain size fixed the number of zero modes present within the Turing zone , and therefore, the number of inhomogeneous branches that exist. For the periodic L=100m domain, only nine zero modes fit within the Turing zone (see Fig. 2.3). Higher wavenumber modes correspond to linearly stable perturbations that decline exponentially.

All the branches obtained with this approach are shown in Fig. 2.4. We now see that the range of rainfall where vegetation is sustained is much wider than expected from the linear analysis. The linear analysis in the previous section predicted the growth of vegetation patterns in the Turing zone, between $1.0\,\text{mm.d}^{-1}$ and $1.25\,\text{mm.d}^{-1}$. The analysis of the full nonlinear system, presented in Fig. 2.4, actually reveals time-invariant pattern equilibria on branches attached to zero modes in the range 0.5 – 1.3 mm.d^{-1}. Although the nonlinear equilibrium may differ in shape from the linear perturbation, it is found that wavenumber n used to perturb the homogeneous equilibrium describes reasonably well the shape of the pattern along the branch obtained from that perturbation. One such equilibrium is displayed for illustration in the top panels of Fig. 2.5. For this particular equilibrium, with wavenumber $n = 2$, the biomass accumulates in two places, and soil water peaks there due to enhanced infiltration rate. Surface water accumulates around those areas.

2.2.2 Stability analysis

Characterizing the stability of equilibria will further help us to understand the dynamics of the system inside the Busse balloon. The Busse balloon is the region

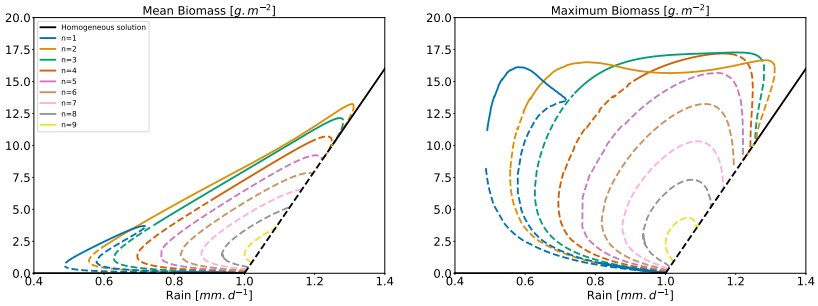


Figure 2.4: *Bifurcation diagram for the Rietkerk's model with $L = 100\,m$. Each branch is labeled by an integer corresponding to the order of the wavenumber associated with the zero mode. Solid lines correspond to stable states and dashed lines to unstable states.*

in the parameter space (κ, R) where at least one stable pattern equilibrium exists. A linear stability analysis gives partial but valuable information about a given solution and its possible evolutions. As we will see in the following, while stable equilibria tend to be the endstate of time evolutions, unstable equilibria may still be relevant for the dynamics. The stability of equilibria is classically estimated based on the Jacobian matrix evaluated at each equilibrium, positive real parts of the eigenvalues signalling instability.

As a first example, the equilibrium for rainfall equal to $0.9\,\mathrm{mm\,d}^{-1}$ of the branch $n = 2$, the associated eigenvalues and the first eigenvector are displayed on Fig.2.5. The majority of eigenvalues have a negative real part. One eigenvalue has a very small, positive real part $(3 \cdot 10^{-10})$, which suggests quasi-neutral stability. Further inspection of the associated eigenvector shows that this quasi-neutrally stable mode is the spatial derivative of the equilibrium pattern. Therefore, it corresponds to a translation mode, which is indeed expected with periodic boundary conditions. Hence, we have a stable pattern which may however translate consistently with the periodic character of the boundary conditions. We therefore attribute the small real part to a numerical artefact (it should be zero) and consider equilibria with positive real part of the highest eigenvalue of the order of 10^{-10} as stable.

This stability analysis is repeated for all the equilibria shown in Fig. 2.4. Stable sections of the branches are drawn as solid lines, and unstable ones as dashed lines. This gives us a more precise idea about what is happening inside the Busse balloon. We now know what the shape of those stable states is, and how and at what rainfall value they lose stability. The existence of multiple stable states for a given value of rainfall is also consistent with previous work based on models and real systems (Bel et al. [2012], Bastiaansen et al. [2018]).

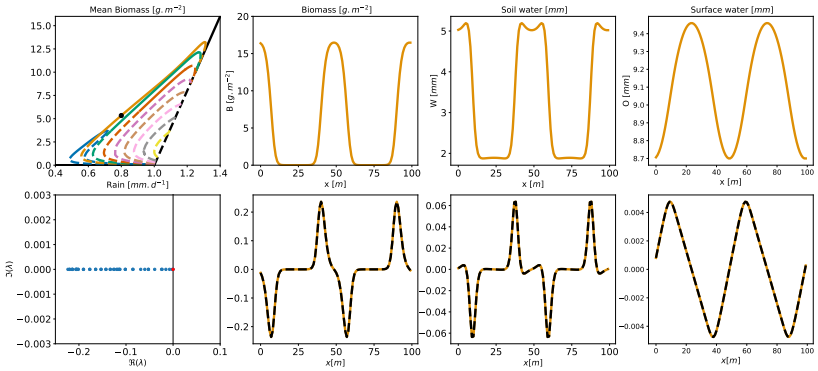


Figure 2.5: *On the upper panels, equilibrium for a given R (rainfall) ($0.9\,mm\,d^{-1}$) on the $n = 2$ branch is shown. The black dot on the left-hand-side panel shows the position of the equilibrium on the bifurcation diagram. The three other panels show, from left to right, B (biomass) [$g\,m^{-2}$], W (soil water) [mm] and O (surface water) [mm]. On the left-hand-side lower panel, eigenvalues of the Jacobian matrix associated with the equilibrium. The real part is on x axis and the imaginary part on the y axis. The larger eigenvalue is represented with a red dot. The black vertical line marks the 0 position. The three other lower panels show, from left to right, the eigenvector associated with the larger eigenvalue projected on B (biomass), W (soil water) and O (surface water) and with a dashed black line, the first spatial derivative of the equilibrium rescaled.*

Some branches of equilibria, such as $n = 5, 6, 7, 8, 9$ are unstable across all their existence domain. Other branches, as $n = 1, 2, 3, 4$, change stability along the branch. These branches of equilibria start as unstable from the low vegetation zero modes on the homogeneous equilibrium. Then, they become stable, and eventually become unstable again shortly before joining the highly vegetated homogeneous equilibrium at the corresponding zero mode. The change in stability may take place at the extreme rain values for which the equilibrium exists, as in the $n = 1$ branch, or at a rainfall value in the middle of a branch. As we know, when a equilibrium loses stability, the real part of one of its eigenvalues changes from negative to positive, which indicates that the equilibrium becomes linearly unstable in the direction of the associated eigenvector. In all of the cases here the change of sign of the eigenvalue happens through zero (as opposed to, through infinity), meaning that, there are zero modes at the intersection of the stable and unstable branch sections. As we show next, this indicates the branching of another branch of equilibrium of the full nonlinear system. A simple way to identify those zero modes is proposed in Appendix A.3.

2.2.3 Mixed states

In the previous section we studied the stability of the "main" branches of equilibria shown in Fig. 2.4. These branches of equilibria originated from the zero modes present on the homogeneous vegetated branch. We also saw that some of these branches of equilibria had zero modes at the intersection of their stable and unstable parts. These zero modes act as bifurcation points from which new branches of equilibria emerge. The latter can be found by starting from the equilibrium at the bifurcation point, perturbed in the direction of the eigenvector associated with the newly positive eigenvalue (zero mode) corresponding to a new unstable direction. Again, a Newton-Raphson iteration allows us to find the new equilibrium. From there, the continuation method explained in the previous section allows us to trace the new branch fully.

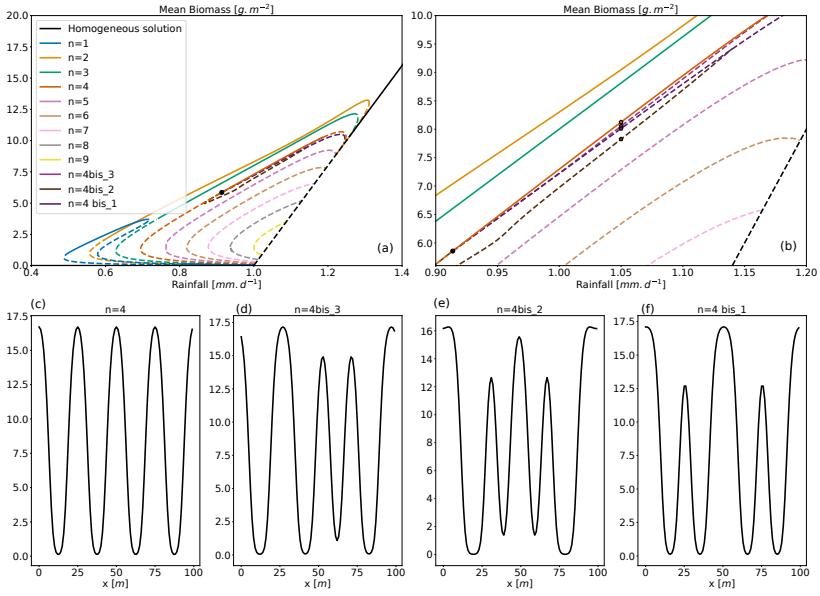


Figure 2.6: *On the left-hand-side upper panel, bifurcation diagram with the addition of mixed state branches. The mixed state branches originating the zero modes along the* $n = 4$ *branch are called* $n = 4bis_1$, $n = 4bis_2$ *and* $n = 4bis_3$. *The bifurcation point is marked with a black dot. On the right-hand-side upper panel, an enhancement of the area around the bifurcation point. On the lower panels, the biomass profile of the* $n = 4$ *and the mixed states for a particular value of rainfall. The position on those equilibria on the bifurcation diagram are marked by circle on the right-hand-side upper panel*

The result of this routine applied to the bifurcation point of the branch $n = 4$ is shown in of Fig. 2.6a and b. At the transition between stability and instability, there are three zero modes. Hence three branches of equilibria start at this transition, as in Fig. 2.6. They all begin at the transition between the stable and unstable part of the $n = 4$ branch and they reconnect with it for higher rainfall. We call those branches $n = 4\,bis_1$,$n = 4\,bis_2$ and $n = 4\,bis_3$. These three branches are close (with regard to the mean biomass) to that of the $n = 4$ branch but if we look closely at their profile (Fig. 2.6c-f) we see how they differ. For a given value of rainfall, the mixed-state equilibria look like a modulation of the $n = 4$ equilibrium by an other wavenumber. Equilibria branching out of zero modes in the homogeneous equilibrium tend to exhibit a single perturbation mode, see Fig. 2.5. By contrast, equilibria branching out of zero modes in those inhomogeneous equilibria exhibit a mixture of modes (lower panels of Fig. 2.6), hence the name "mixed states".

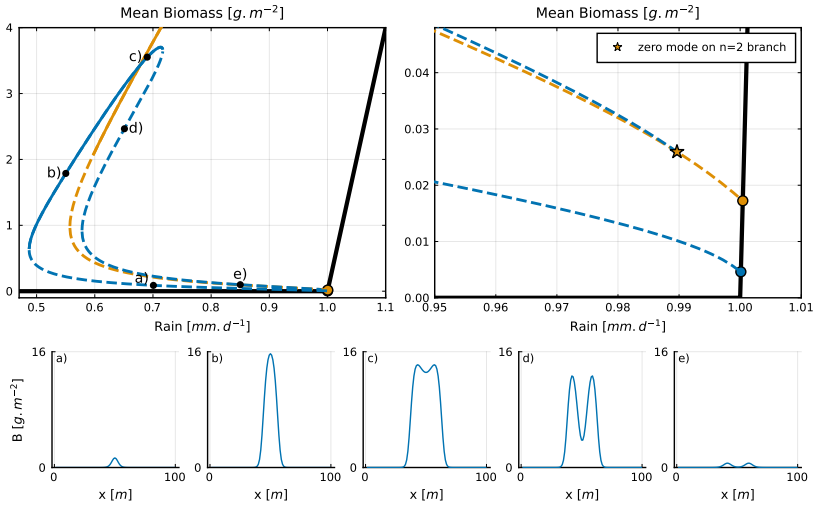


Figure 2.7: *A focus in the bifurcation diagram on the $n = 1$ and $n = 2$ branches; the stable (unstable) states are noted with a continuous (dashed) line. Upper right-hand-side panel, a zoom-in on the area of the bifurcation diagram where the $n = 1$ branch connects with the $n = 2$ branch. This connection is represented by a star. In panels (a-e), equilibria along the $n = 1$ branch are shown. Each corresponds to a black dot in the upper left-hand-side panel.*

The equilibria along the mixed-state branch $n = 4\,bis_3$ are unstable, with positive eigenvalues. The branches $n = 4\,bis_2$ and $n = 4\,bis_3$ reconnect around $1.14\,\mathrm{mmd}^{-1}$. There are numerous mixed-state branches, obtained from the different zero modes at bifurcation points found along the main branches. These can

also be found to emerge from zero modes present on the unstable sections of the main branches.

For example, in the low vegetated unstable part of the $n = 3$ branch (see Fig. 2.8), we find two zero modes at the same value of rainfall, from which two mixed state branches emerge: one labelled $n = 2\,bis$ because it connects to the $n = 2$ branch and one labelled $n = 3\,loc$ which connects to the $n = 4$ branch. The $n = 3\,loc$ refers to the fact that the equilibrium of that branch is localized in space. The $n = 1$ main branch is special in two ways. Firstly, as Zelnik et al. [2013] stated, it is the only stable localized state. Second, it starts from a zero mode on the homogeneous equilibrium, but it ends up connecting to the $n = 2$ branch as if it was a mixed state, see Fig. 2.7. The evolution of the shape along this branch goes from one localized vegetation peak in the stable part to two localized vegetation peaks in the unstable part close to the connection with the $n = 2$ branch.

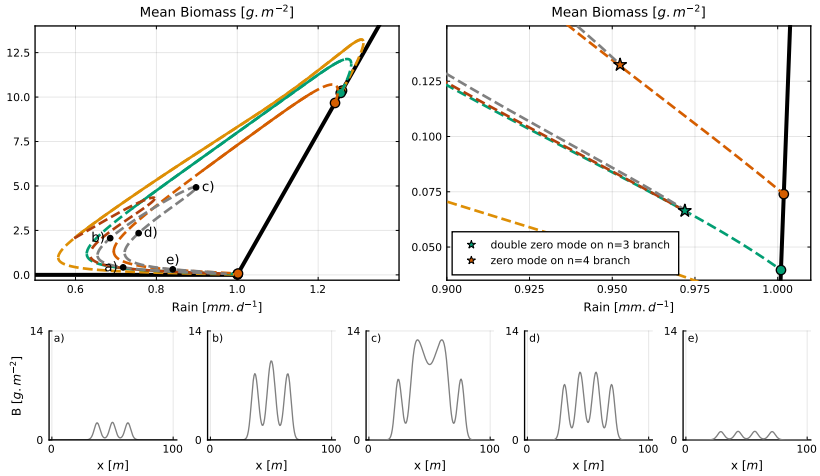


Figure 2.8: *A focus on the bifurcation diagram on the $n = 2$, $n = 2\,bis$, $n = 3$, $n = 3\,loc$ and $n = 4$ branches; the stable (unstable) states are noted with a continuous (dashed) line. In the upper right-hand-side we show a zoom-in of the bottom part of the bifurcation diagram. The $n = 3$ branch exhibits a double zero-mode, indicated by the green star. Two equilibria emerge from that double-zero mode, the $n = 2\,bis$ and the $n = 3\,loc$. The $n = 3\,loc$ branch is characterized by a three-bump solutions which is localized. The first equilibrium, connects with the $n = 2$ branch while the second one connects with the $n = 4$ branch at the zero mode indicated by the orange star. In panels (a-e), equilibria along the $n = 3\,loc$ branch are shown. Each corresponds to a black dot in the upper left-hand-side panel.*

All mixed-state branches share similar characteristics, with states appearing as a modulation of a main branch. Even though they are unstable, we expect mixed-state equilibria to influence the dynamics of nearby trajectories, depending on the value of the positive eigenvalue.

2.3 Numerical simulations of trajectories

To assess the relevance of the bifurcation diagram for understanding transient dynamics, we performed two series of numerical simulations.

2.3.1 Trajectories in a changing environment

In order to assess the relevance of the various branches for the dynamics, we propose the following numerical experiment. The Rietkerk model is run with rainfall changing over time at a rate of $\frac{dR}{dt} = -5.10^{-6}\,\mathrm{mm\,d^{-2}}$. The starting point is the vegetated homogeneous equilibrium with rainfall $R = 1.4\,\mathrm{mm\,d^{-1}}$. The final rainfall is $0.5\,\mathrm{mm\,d^{-1}}$. The result is shown in Fig. 2.9.

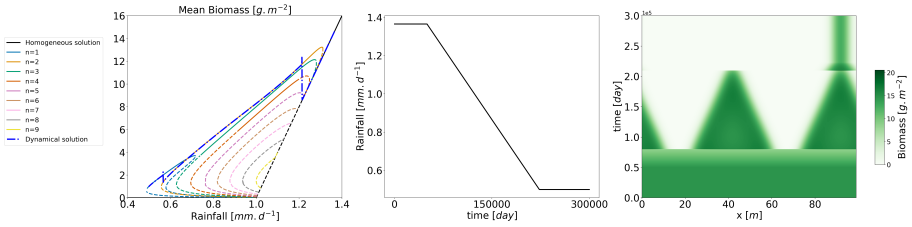


Figure 2.9: *Trajectory of the Rietkerk model under a decreasing rainfall scenario. On the left panel, the trajectory in the bifurcation diagram plotted in blue dashed-dot line. On the middle panel, the rainfall with respect to time and on the right panel, the time evolution of the biomass.*

Until $R \sim 1.2\,\mathrm{mm\,d^{-1}}$, the system stays in homogeneous equilibrium. At this point, the system undergoes a subcritical Turing bifurcation and jumps to an heterogeneous equilibrium. The patterned branch on which the system lands is the $n = 2$ branch. After that, the system tracks the $n = 2$ branch until this equilibrium loses its stability. Finally, the system switches to the only other stable equilibrium, the $n = 1$. For this experiment, the mixed states do not have an influence on the trajectory. But in the following we will see that even if the mixed states are unstable, they can still play a role in the dynamics.

2.3.2 Effect of a mixed state on trajectories

Here we address the question of whether unstable mixed-state equilibria are also able to influence system-transient trajectories. In this case the rainfall is set to rainfall $R = 1.05\,\mathrm{mm\,d}^{-1}$, for which a mixed-state equilibrium exists.

The initial condition is an unstable equilibrium, $n = 5$, with a small perturbation along the direction of the first eigenvector. Fig. 2.10a and b summarize the evolution of the biomass pattern over time and the corresponding trajectory in a summary phase space. This summary phase space consists of a two-dimensional phase space where the two dimensions are the mean biomass and the maximum biomass. With that in mind, we observe that the system leaves the $n = 5$ unstable equilibrium by first reorganizing itself: mean biomass remains constant while maximum biomass increases. This means that one or more vegetation bumps are growing at the expense of others. After that initial reorganization, an excursion on higher mean and maximum biomass takes place. It is during this out-of-equilibrium excursion that one of the vegetation bumps is lost. At this point in time, the vegetation profile, containing four vegetation bumps, passes close to the three mixed states originating from zero modes on the $n = 4$ branch identified in the previous section. Then the system undergoes an other transition to the $n = 3$ equilibrium. To have a better representation of this trajectory, we also show the time evolution in Fig. 2.10b. We see that the system quite slowly leaves the $n = 5$ unstable equilibrium. The state is indeed unstable, but the associated positive eigenvalues are small, such that the dynamics around the equilibrium are slow. After abruptly departing from the $n = 5$ equilibrium, one biomass bump disappears, leading to a rearranged state with four bumps. The biomass profiles at three points in time are represented in Fig. 2.10c-e, and their corresponding position are also shown in panel a. In each of panels c-f, the shape of the $n = 4bis_3$ mixed state is also shown. The shape of the dynamical solution is actually close to the $n = 4bis_3$. That equilibrium is unstable, but the system lingers in its vicinity for a considerable period of time before another bump of biomass vanishes, propelling the system towards the stable equilibrium of $n = 3$.

Switching from one state to an other by losing one or more vegetation bumps is a known feature of vegetation pattern models (Bastiaansen and Doelman [2019], Bastiaansen et al. [2020]). This mechanism is similar to the sideband instability (Doelman et al. [2012], Siteur et al. [2014b]) eventhough this is only defined for an infinite domain. We used the same setup with different rainfall values along the $n = 5$ branch. The fact that the system passes close to a mixed state is consistent along the $n = 5$ branch alone for values of rainfall for which mixed-state equilibria exist. For rainfall lower than $\sim 0.91\mathrm{mm/d}$, the system jumps directly to the $n = 3$ equilibrium. Now if we consider the same rainfall but we start from an other unstable branch like the $n = 6$ or $n = 7$, the dynamics is different. For $n = 6$, we

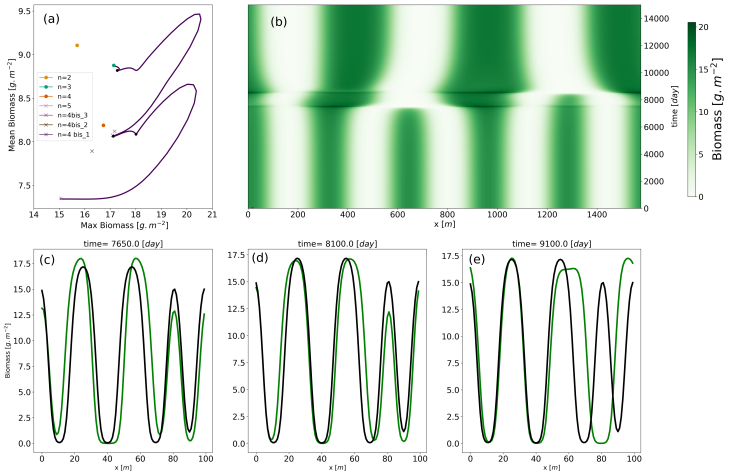


Figure 2.10: *On the left upper panel, trajectories on a summary phase space from an initial condition close to the $n = 5$ equilibrium with a fixed rainfall $R = 1.05\, mm\, d^{-1}$. The relevant equilibria are shown, the stable equilibria are represented with a circle and the unstable equilibria with a cross. On the right panel, we show the time evolution of the biomass. On the three lower panels, the dynamical solution at three different times is represented (in green) and also the shape (in black) of the mixed state denoted by $n = 4bis_3$.*

observe a different type of destabilization similar to a period doubling (Doelman et al. [2012], Siteur et al. [2014b]) for an infinite domain. With that mechanism the system transitions to the $n = 3$ equilibrium without passing through a mixed state, and the system spends less time around the unstable equilibrium of $n = 6$ compared to the $n = 5$ case. This might be explained by the fact that the positive eigenvalue on the $n = 6$ is larger than the one on the $n = 5$ solution. For $n = 7$, the transition is even more rapid, as expected for an even larger positive eigenvalue, but the landing point is still $n = 3$. In that case, we observe a destruction of four bumps similar to a sideband instability.

2.4 Discussion

We uncovered the existence of mixed states in Ritkerk's model and showed their importance for transient dynamics. As far as we are aware, such mixed states have never been identified nor described in models for vegetation patterns.

Mixed states emerge at the transition between unstable and stable states along a branch of equilibria, and have a functional form that appears as the combination of two equilibria from the main branches. We found that while these equilibria

are unstable, they may still influence the system's dynamics by slowing down its evolution when it passes near them.

The influence of unstable modes on dynamics has been studied in ecological models. For example, Sherratt et al. [2009] showed how spatio-temporal chaos appears in the wake of an unstable wave train for the complex Ginzburg-Landeau equation. In the more general context of ecology, Hastings et al. [2018b] and more recently Morozov et al. [2020b] proposed a classification of transient phenomena in ecological models based on a dynamical system approach. In their definition a dynamical regime is transient if it persists for a sufficiently long time (quasi-stable) and if the transition between two regimes occurs on a much shorter timescale than the time of existence of the quasi-stable regime. According to that definition, the behaviour observed in section 2.3.2 can be seen as a transient phenomenon. Indeed, the systems spends hundred to thousands of days around unstable equilibria ($n = 5$, $n = 4bis_1$ and $n = 4bis_3$) and it takes only a few days to jump to the final stable equilibrium. By following the typology presented in those two papers, the transient state observed here can be qualified as a 'crawl by' transient. Indeed the transient observed is linked to the existence of a saddle-type invariant set: the mixed state. Transient dynamics have also been studied in the context of coexistence in vegetation patterns by Eigentler and Sherratt [2019] and are characterized by the small size of a positive eigenvalue. Long transients can also be observed in very slow front invasion dynamics [Van De Leemput et al., 2015] The mechanism behind the transient is different but the effect is the same: the system spends a long time in a region of the phase space without an attractor.

As we see in section 2.3.2, the history and the initial conditions of the system are important to see whether the mixed state will or will not appear in the dynamics. Other vegetation pattern models exhibit this type of sensitivity to history and initial conditions (Sherratt [2013], Adams et al. [2003] and Alberti et al. [2015]). Further research is needed to determine whether mixed states are a common feature of reaction-diffusion systems.

We adopted periodic boundary conditions, as in previous studies (Rietkerk et al. [2002a], Dekker et al. [2007]). As stated by Dijkstra [2011], the periodic boundary conditions allow for the existence of unstable equilibria with a high wavenumber. However, this boundary condition, widely used in reaction-diffusion models due to its simplicity and convenience, may not reflect real-world scenarios accurately. More generally, working with a periodic domain discretizes the set of admissible equilibria. Hence, the significance of mixed states for describing the dynamics of non-periodic infinite-size systems needs to be further assessed.

As a step towards this objective, we computed the bifurcation diagram for a larger domain size of $L = 200\,\mathrm{m}$, instead of $L = 100\,\mathrm{m}$. The result is shown in Fig. 2.11. As expected, we observed more branches in this case but, remarkably, the branches and the stability of the branches shared between the two domains are

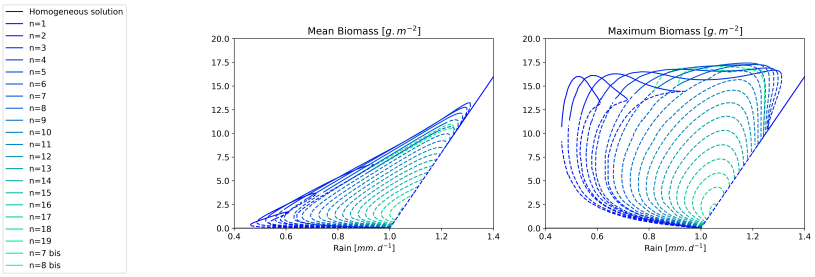


Figure 2.11: *Bifurcation diagram for the Rietkerk's model with $L = 200$ m. Each branch is labeled by an integer corresponding to the order of the wavenumber associated with the zero mode. Plain lines correspond to stable states and dashed lines to unstable states.*

the same as for $L = 100$ m. Of course the even n number branches for the $L = 200$ m domain are the same as for the $L = 100$ m domain. The new branches are all designated with an odd n number as a consequence of the extended domain. The range of rainfall that can support a stable vegetation pattern also increased slightly with the larger domain size, with the $n = 1$ branch extending this range.

These findings suggest that the existence of mixed states and their stability properties is robust across domain sizes, even though how they will manifest themselves in continuous large domains is still to be established.

2.5 Conclusions

We present an in-depth analysis of the Rietkerk model's behaviour that we believe sheds a new light on the dynamics of vegetation patterns. Our analysis is based on the bifurcation diagram of the vegetation pattern model, which we constructed using a variety of techniques. First, we performed a linear stability analysis of the homogeneous equilibrium of the system, which allowed us to delineate the so-called Turing zone. This zone is characterized by the instability of the homogeneous equilibrium to small heterogeneous perturbations, and it serves as a starting point for our analysis. Next, we used perturbed states at the edge of the Turing zone, the so-called zero modes, to construct whole branches of equilibria associated with the system. To obtain these branches, we used a continuation method based on the Newton-Raphson algorithm. By doing so, we were able to obtain the heterogeneous equilibria for a given size of the domain. As expected, due to the system's nonlinearity, we discovered that the system allows for multiple equilibria for a given value of a parameter, specifically rainfall. We went a step further by assessing the stability of those equilibria by computing the eigenvalues and associated eigenvectors of the Jacobian matrix. This stability analysis showed

that inhomogeneous vegetated states can exist and be stable, even for a values of rainfall for which no vegetation exists in the non-spatialized system. Yet, we also found that the main branches of equilibrium originating from a zero mode are not the only ones present in the system. At the transition between unstable and stable states along one branch, a new type of equilibrium appears. These latter types of equilibria, which we called mixed states, are always unstable equilibria and they appear as a mix of two equilibria from the main branches. Although these equilibria are unstable, they affect the dynamics by slowing down the evolution of the system when it passes close to it. This slowing effect has been described in ecology, but to the best of our knowledge, the mixed-state influence on the dynamics had not been previously shown for vegetation patterns. Overall, our approach allowed us to construct a bifurcation diagram that gives us valuable insights about the behaviour of the system. This approach is helpful to disentangle the fate of the system in the Busse balloon and could be used to assess the existence or non-existence of mixed states in spatially extended systems.

3

Rate-induced transitions and noise-driven resilience in vegetation pattern dynamics

This chapter is based on the following paper in open discussion (NPG):
Vanderveken, L. and Crucifix, M. (2024): Rate-induced transitions and noise-driven resilience in vegetation pattern dynamics, *Nonlinear Processes in Geophysics*.

Abstract

Understanding the resilience and stability of vegetation patterns under changing environmental conditions is crucial for predicting ecosystem responses to climate change. This study investigates the dynamics of vegetation patterns in response to a spatially homogeneous decrease in rainfall across the entire domain. Starting from high rainfall with a stable homogeneous vegetated state, we applied various rates of rainfall reduction to observe system transitions. We find that rainfall decrease may cause transitions to two or three pulse states, or abrupt shifts to bare soil depending on the rate of change, highlighting the significance of rate-induced tipping (R-tipping) in open dynamical systems.

We identified the pulse destruction timescale ($\tau_{\text{destruction}}$) and the rearrangement timescale (τ_{rear}) as the critical timescales which govern the system response to gradual environmental changes. The rearrangement timescale, significantly longer than $\tau_{\text{destruction}}$, is relevant for characterizing the system behaviour under slow perturbations. Dimensional analysis and sensitivity analysis with numerical experiments further validate the fundamental connections between these timescales.

Additionally, we examined the impact of spatially and temporally structured noise on vegetation pattern resilience. Perturbations modelled as Gaussian stochastic processes with specific autocorrelation structures were applied to the system. We find that increased spatial autocorrelation in noise reduces pattern formation, while temporal autocorrelation at critical timescales significantly influences biomass mean and variance. The co-existence of multiple equilibria and unstable states, combined with the presence of ghost attractors enhances system resilience by providing alternative stable configurations under fluctuating conditions.

These findings underscore the importance of considering slow timescales and structured noise when analyzing vegetation dynamics. Understanding these factors is essential for predicting ecosystem resilience and developing strategies to manage vegetation systems under climate variability.

3.1 Introduction

Understanding the dynamics of vegetation patterns under varying environmental conditions is crucial for predicting ecosystem responses to climate change. Vegetation patterns, such as the regular arrangement of plant patches, arise from complex interactions between biological processes and environmental factors [Klausmeier, 1999a]. These patterns are particularly sensitive to changes in environmental conditions [Gilad et al., 2007], which directly affect, for example, water availability, a critical resource for plant growth in semi-arid regions [Deblauwe et al., 2008]. Therefore, investigating how vegetation systems respond to different perturbations can provide valuable insights into their resilience and stability.

The seminal works by Holling [1973] established the difference, in ecology, between stability and resilience. Stability refers to the ability of a system to return to its equilibrium after a perturbation and is linked to the eigenvalues associated with a given stable equilibrium. Resilience defines the ability of an ecosystem to maintain its function. For example, in semi-arid areas, an ecosystem constrained by limited water supply may achieve its highest biomass when vegetation is distributed in the form of patterns. Furthermore, based on vegetation models, we know that different pattern configurations may be compatible with a same boundary condition (von Hardenberg et al. [2001], Dijkstra [2011], Zelnik et al. [2013]). As these different configurations may all achieve high biomass, it is generally conjectured that resilience is effectively enhanced by the multiplicity of possible patterns.

However, understanding resilience also requires attention to the nature of the perturbation [Kéfi et al., 2019]. A system may react very differently depending on the type of perturbation being applied to it.

Our objective is to determine the critical scales, in time and space, which determine the response of the system to environmental perturbations. We consider, at first, linear, deterministic perturbations such as a linear decrease in precipita-

tion, and then stochastic perturbations. We aim at establishing general principles. Even though the work is based on a specific numerical model of vegetation [Rietkerk et al., 2002a], we aim at identifying which critical time scales emerge from the model construction, and how they influence the response of the system.

To this end, we follow the framework established by previous studies. More specifically, Siteur et al. [2014b], Chen et al. [2015] and Sherratt [2013] showed the importance of the rate of change and noise; Bastiaansen et al. [2020] identified in Klausmeier's vegetation patterns model a critical time scale for which the patterns do not have the time to adapt to the environmental change. All those works emphasize the importance of understanding rate-induced transitions.

After those studies, a number of questions remain: are there more than one critical time scale in a vegetation pattern model; what is the impact of those internal timescales, and can they be linked to parameters of the model? In the following, we will show how these critical timescales manifest themselves in Rietkerk's model [Rietkerk et al., 2002a], and how they influence both the response to deterministic and stochastic perturbations, with emphasis on the possible occurrence of a resonance process.

3.2 Model description

As announced in the introduction we use the vegetation model by Rietkerk et al. [2002a]. As is common for reaction-diffusion models, it combines two mechanisms for creating patterns: local facilitation, and long-range inhibition. Local facilitation is caused by the water infiltration feedback. It is based on the idea that in a semi-arid region the soil crust effectively prevents water infiltration. The presence of biomass and more specifically the roots associated with this vegetation increases the water infiltration by drilling the soil crust. Long-range inhibition is caused by rapid diffusion of surface water preventing the accumulation of water in some places of the spatial domain and so the creation of biomass. The presence of these two processes places the Rietkerk's model in the category of scale-dependent feedback model (Lefever and Lejeune [1997], Rietkerk and van de Koppel [2008b], Van De Koppel et al. [2006]). Although models of this class are known to produce regular patterns as stable equilibria, Vanderveken et al. [2023] showed that non regular equilibria (mixed states) exist and play a role in the dynamic of the system despite its instabilities. Another class of pattern-formation models have been proposed recently by Siteur et al. [2023]. This class of models is based on density-dependent-aggregation of biotic or abiotic species and can create non regular patterns.

Three variables are modelled in Rietkerk's model: Biomass (B) [g.m^{-2}], soil water (W) [mm] and surface water (O) [mm]. They respond to the following system

of partial differential equations:

$$\begin{aligned}
\frac{\partial B}{\partial t} &= c g_{max} \frac{W B}{W + k_1} - dB + D_B \Delta B, \\
\frac{\partial W}{\partial t} &= \alpha O \frac{B + k_2 w_0}{B + k_2} - g_{max} \frac{W B}{W + k_1} - r_w W + D_W \Delta W, \\
\frac{\partial O}{\partial t} &= R - \alpha O \frac{B + k_2 w_0}{B + k_2} + D_O \Delta O,
\end{aligned} \tag{3.1}$$

where Δ is the Laplacian operator and R the rainfall [mm.d^{-1}]. Rainfall is the external forcing of the system which we consider to be a spatially-independent function. The first term in the biomass equation represents water uptake by the plant. The first term in the soil water equation is linked to the infiltration rate of water in the soil that is enhanced by the presence of biomass. The factors in front of the Laplacians (ΔB, ΔW and ΔO) represent the diffusion constants of the different quantities. We consider a periodic domain of size $L = 100$m. The parameters are the same as in chapter 1.

3.3 Effect of rainfall perturbation on vegetation dynamics: identifying critical timescales

We consider a spatially homogeneous perturbation applied to surface water, representing a decrease in rainfall across the entire domain. This type of perturbation is meaningful as it mimics gradual shifts in climate means. By applying different rates of change to a system that is initially in a high rainfall state, we aim at identifying which critical factors influence the transient response of vegetation. In this context, rainfall is said high when it induces a stable, fully vegetated state.

Previous research has highlighted the dependence of system solutions on the rate of environmental change, as common in open dynamical systems. In the context of vegetation patterns, different rates of rainfall decrease can lead to diverse outcomes, ranging from transitions to multi-pulse states to abrupt shifts to bare soil.

Starting from a high mean rainfall situation ($R = 1.4$mm.day^{-1}), for which only the homogeneous vegetated state is stable, we decrease rainfall with different rates of change a ([mm.day^{-2}]). Fig. 3.1 shows the evolution of the spatial structure of the biomass (in green) as a function of rainfall, for different values of a. We find a transition from an homogeneous state to a heterogeneous distribution with two or three vegetation 'pulses', before it finally disappears. The sequence and timing of the transitions depend on a. For a rate of change of 10^{-3} mm.day^{-2} the system jumps directly from a homogeneous vegetated state

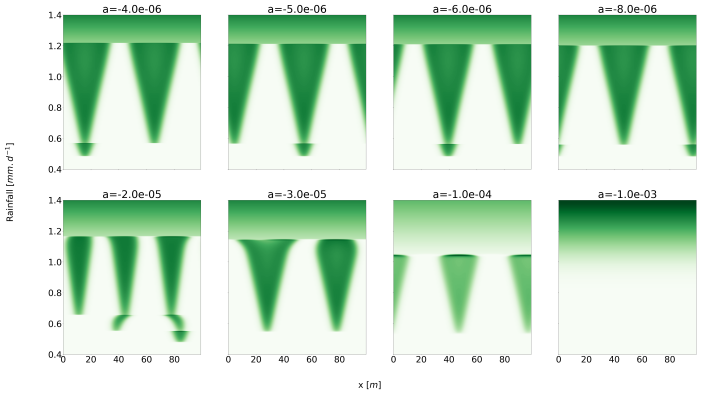


Figure 3.1: *Sensitivity of Rietkerk's model to various rates of change in the rainfall. Each panel represents a solution with a given rate of change a. The x-axis is the spatial dimension, and y-axis the rainfall. Every run has the same starting and ending point rainfall values but they differ by the rate of change. Every simulation starts with a homogeneous vegetated state which is the only stable equilibrium at this value of rainfall. For the last value of rainfall ($R = 0.4$mm.days^{-1}), the only stable equilibrium is the homogeneous bare soil solution.*

to a bare soil solution. The critical rate of change at which all vegetation is eradicated is $\tau_{R_{\text{tip}}} \sim 1000$ days.

It is not surprising that the response depends on the rate of the perturbation change. Ashwin et al. [2012] established general principles of so-called rate-induced tipping (R-tipping) in models based on ordinary differential equations, and rate-dependent responses were also described specifically in models of vegetation patterns (Siteur et al. [2014b], Chen et al. [2015], Bastiaansen et al. [2020]). However, the value of $\tau_{R_{\text{tip}}}$ is intriguing. Indeed, the timescale associated with the destruction of vegetation pulses is, through dimensional analysis, estimated to be $\tau_{\text{destruction}} = \frac{\alpha}{c\, g_{max}} \left(\frac{R}{k_2\, g_{max}}\right)^3 \frac{1}{d} = 52$d.

This relationship is linked to the transfer of water to biomass, to vegetation mortality and to rainfall. To test the dependence of the proposed scaling on rainfall, we conducted the following numerical experiments. Starting from a stable equilibrium consisting of two vegetation pulses at $R = 1.2$mm.day^{-1}, we reduced abruptly the rainfall to values between 0.3mm.day^{-1} and 0.8mm.day^{-1}. This reduction leads to vegetation collapse, driving the system toward the bare soil equilibrium. We then determined the destruction timescale by fitting an exponential function to the mean biomass evolution for different rainfall values. The resulting timescales are shown

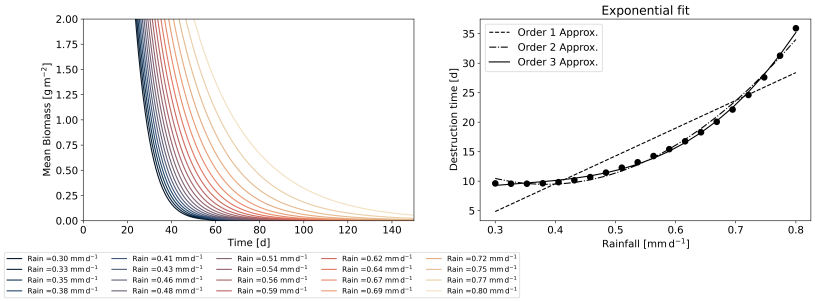


Figure 3.2: *The left panel shows the mean biomass over time for rainfall values ranging from* 0.3*mm.day*$^{-1}$ *to* 0.8*mm.day*$^{-1}$*. The right panel displays the destruction timescales obtained from an exponential fit as a function of rainfall, along with polynomial fits of the destruction timescale of orders one, two, and three.*

in the right panel of Fig. 3.2. Our results reveal a cubic relationship between the destruction timescale and rainfall, supporting the validity of our scaling.

Having $\tau_{R_{\text{tip}}}$ about 30 times $\tau_{\text{destruction}}$ suggests that a slower process dominates the behaviour of the system under changing environmental conditions. Bastiaansen et al. [2020] already identified another critical timescale within the Klausmeier's model (Klausmeier [1999b]). It is linked to the movement of pulses towards a stable, regular state. This concept is crucial for understanding vegetation dynamics in response to gradual environmental changes.

We now proceed to determine a similar time scale in Rietkerk et al. [2002a]'s model, and will call it the rearrangement timescale, τ_{rear}. First, we perform a numerical experiment where a pulse is removed for a given rainfall value, and the time taken for the system to stabilize is computed. Fig. 3.3 shows the results for different values of rainfall. We find that $\tau_{\text{rear}} \sim 1000$ days. This rearrangement timescale is of the same order as $\tau_{R_{\text{tip}}}$, suggesting a fundamental connection between the two. This correspondence would also support that R-tipping is conditioned by the slowest timescale in the system. The rearrangement timescale effectively represents this slowest process, dictating the system's overall response to changing conditions. Second, we attempt to link this rearrangement timescale to quantities in the system.

Inspired by the scaling proposed in Bastiaansen and Doelman [2019], we reason on the fact that the movement of pulses are determined by diffusion coefficients. Specifically, we take advantage of the fact that the ratio between the slow and the fast diffusion coefficients in the reaction-diffusion model drives the creation of the patterns (Murray [2003],Meron [2015]). For Rietkerk's model the fast component is the surface water (O) and the slow components are the biomass (B) and

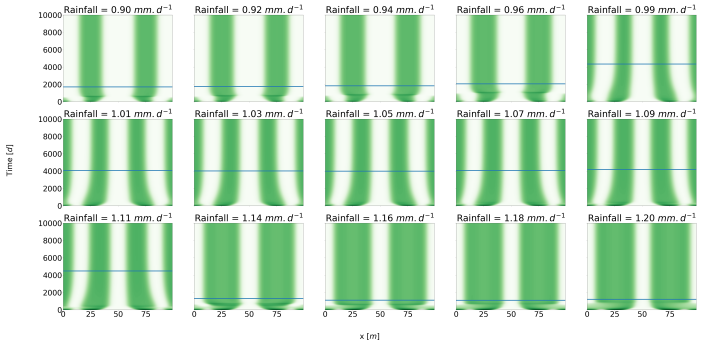


Figure 3.3: *Rearrangement time scale with respect to the rainfall. Each panel represents the solution of the following numerical experiments, we start in the stable equilibrium with four pulses and we remove one pulse. We then identify for each experiment the time until the system reaches a new equilibrium by moving around the pulses. This time is shown by a horizontal blue line on each panel.*

the soil water (W). Hence, we propose the following scaling for the rearrangement time $\tau_{rear} = \frac{\alpha}{c\, g_{max}} \left(\frac{R}{k_2\, g_{max}}\right)^3 \frac{1}{d} \sqrt{\frac{D_O}{D_B}} = 1000$d. The key factor determining the rearrangement time appears to be the square root of the ratio between the diffusion coefficients of the fast and slow variables. To verify this, we perform a series of experiments where the diffusion coefficient of the slow variables (biomass and soil water) varied by a factor f. To obtain a stabilization time for the different values of f, we run a series of numerical experiments similar to the one presented earlier. We start from a stable state for a given value of rainfall and f, then we remove one pulse of vegetation. We compute this stabilization time for different values of rainfall and took the larger stabilization time because it is the one that is of interest regarding R-tipping. The results are presented in Fig. 3.4. The rearrangement timescale which is diagnosed numerically fits the theoretical curve proposed for τ_{rear} fairly well.

This finding highlights the critical role of the rearrangement timescale in determining the system's response to environmental changes. Specifically, it emphasizes the need to account for this slower timescale when analyzing vegetation dynamics. Understanding and quantifying this timescale provides valuable insights into the resilience and stability of vegetation systems under gradual environmental shifts.

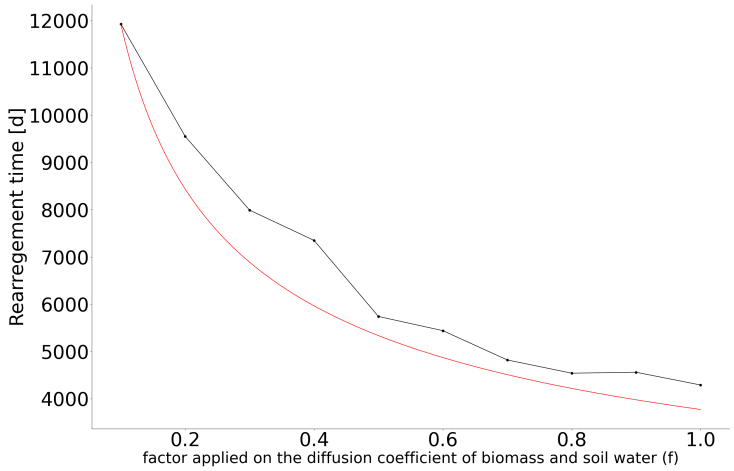


Figure 3.4: *Link between the factor f applied on the diffusion coefficient of the the "slow" components (biomass and soil water) and the rearrangement timescale. This timescale is estimated by finding a stable equilibrium for the new diffusion coefficients, remove one of the pulse and then estimate the stabilization time. This procedure is applied for different values of rainfall and we take into account the largest stabilization time. The rearrangement times obtained with this methed are the black dots and the red line is a visual indication that scales as $\frac{1}{\sqrt{x}}$.*

3.4 Effect of Spatially and Temporally Structured Noise on Vegetation Pattern Resilience

The kind of perturbations applied to the system is an important aspect of resilience diagnosis (Kéfi et al. [2019]) and specifically, the spatial scale of the perturbation must be considered. To explore the effect of the spatio-temporal structure of the perturbation applied to the system, we apply an additive noise with a temporal structure on surface water. This temporal structure is characterized by a temporal autocorrelation. A high temporal autocorrelation implies a slower change in the precipitation. We also add an additive structured noise with a fixed temporal autocorrelation of one day on biomass to represent the effect of external factor such as grazing. It is not the most realistic that could be applied to biomass but we used it for the sake of simplicity. In the following section, we consider a dynamic perturbation consisting of a spatially distributed noise modeled mathematically as a Gaussian stochastic process with mean $\mathbb{E}[\xi(t,x)] = 0$ and standard deviation $\sigma = 0.1$. The temporal structure is that of an Orstein-Uhlenbeck process. The correlation function is $\mathbb{E}[\xi(t,x)\xi(s,y)] = e^{-|t-s|/\lambda_t} e^{-(x-y)^2/\lambda_s^2}$.

Stochastic perturbations are applied to the biomass B and surface water W. Formally, the model takes the form of:

$$\begin{aligned}
\frac{\partial B}{\partial t} &= c g_{max} \frac{W B}{W + k_1} - dB + D_B \Delta B + \xi_B(x,t), \\
\frac{\partial W}{\partial t} &= \alpha O \frac{B + k_2 w_0}{B + k_2} - g_{max} \frac{W B}{W + k_1} - r_w W + D_W \Delta W, \\
\frac{\partial O}{\partial t} &= R - \alpha O \frac{B + k_2 w_0}{B + k_2} + D_O \Delta O + \xi_O(x,t).
\end{aligned} \tag{3.2}$$

where $\xi_O(x,t)$ and $\xi_B(x,t)$ are independent noise processes. We used the same numerical scheme as explained in the appendix of chapter 1 -for the deterministic part- and we propagated the stochastic part with a Euler-Maruyam scheme. For biomass, we consider an autocorrelation timescale of one day, and different autocorrelation length-scales ($\lambda_{biomass,s}$) are tested. For surface water, the perturbation is homogeneous in space and different autocorrelation timescales $\lambda_{rainfall,t}$ are tested.

Fig. 3.5 summarizes the stationary response of the model to $\lambda_{biomass,s}$ and $\lambda_{rainfall,t}$, considering the mean biomass. Outputs reported on those tables is the average of 15 experiments. First, we consider the spatial structure of the noise, applied to the biomass. We focus on the horizontal lines of the tables, one by one, with the structure of the perturbation changing from highly heterogeneous to almost homogeneous as each line is browsed from the left to the right (increasing $\lambda_{biomass,s}$) We find that mean biomass tends to decrease as spatial autocorrelation increases, and this occurs regardless of the choice of time autocorrelation. This suggests that more homogeneous stochastic perturbations tend to destroy more biomass and send the system towards the bare soil equilibrium. The resilience of the vegetation is thus reduced if the perturbation is spatially more homogeneous.

Second, we now focus on the time-correlation of the stochastic perturbation of surface water. We find that both the spatial mean *and* the variance reach a minimum at $\lambda_t = 10$d. This timescale is the $\tau_{\text{destruction}}$ timescale previously identified by the scale analysis. This suggests a form of resonance associated with $\tau_{\text{destruction}}$ preventing self-organisation of vegetation. On the other hand, biomass reaches a maximum for a perturbation time scale of 1000 days, coinciding with the rearrangement timescale τ_{rear} that we also identified by the scaling analysis.

To visualise the behaviour for those different values of temporal autocorrelation, we show, in Fig. 3.6, realizations representative of the general behaviour, for four values of λ_t. We see that patterns tend to disappear for $\lambda_t = 10$d and reappear for $\lambda_t = 1000$d. The ability of the system to maintain or not patterns, depending on the time scale of the perturbation, explains the variation of mean biomass observed in Fig. 3.5. We suggest that the slow stochastic perturbation is

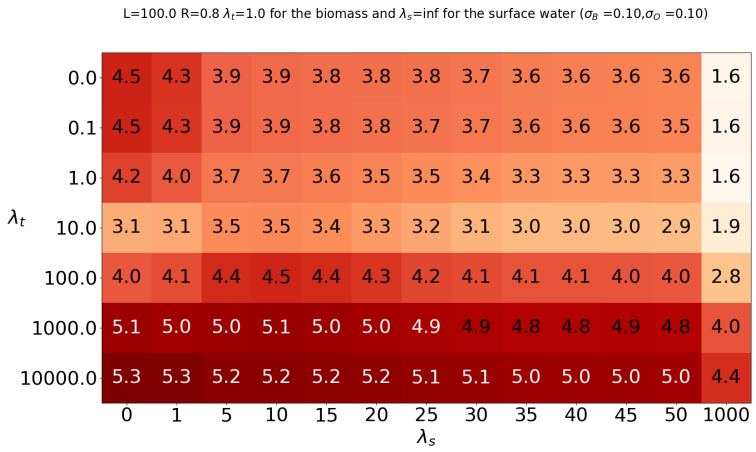


Figure 3.5: *Summary table for the runs with stochastic forcing. For each cell, we ran the model 15 times with the same λ_t and λ_s. The table indicates the ensemble mean of the temporal mean of the spatial mean.*

more effective at moving the system gently around the states associated with the highest biomass, without destroying patterns. The slow timescale (rearrangement timescale) is intrinsically linked to the spatial extension of the model. It would not exist in a zero-dimensional analysis. In this respect, we have noted already that nonlinear, spatially extended systems tend to have multiple equilibria for a given input - here, a given rainfall. The multiplicity of equilibria, whether they are stable or not, increases the resilience of the system in the sense of Holling [1973]. Metaphorically, such equilibria may be seen as tree branches in a forest to which an orangutan might cling to to avoid falling.

This phenomenon is clearly visible in Fig. 3.7, displaying the time evolution of the biomass with a fixed rain fall of 0.8mmd^{-1}. In this configuration, we see that the system jumps from a pulse configuration to an other, passing from two to three pulses or vice versa. The transition, associated with the vanishing or the creation of a pulse, happens quickly, with a time scales of a few days. We find again the τ_{pulse} (fast) timescale identified earlier. Those configurations correspond to stable equilibria for the chosen rainfall as previously identified (Zelnik et al. [2013], Vanderveken et al. [2023]). The two and three pulse configurations are not the only states being visited by the system. From time to time a big pulse associated with a small pulse configuration appears. The latter does not correspond to an equilibrium for a rainfall value of 0.8mmd^{-1}, but it can be interpreted as the ghost of a *mixed state* identified in Vanderveken et al. [2023]. Mixed states are always unstable and exhibit pulses with different heights. The mixed state that interests

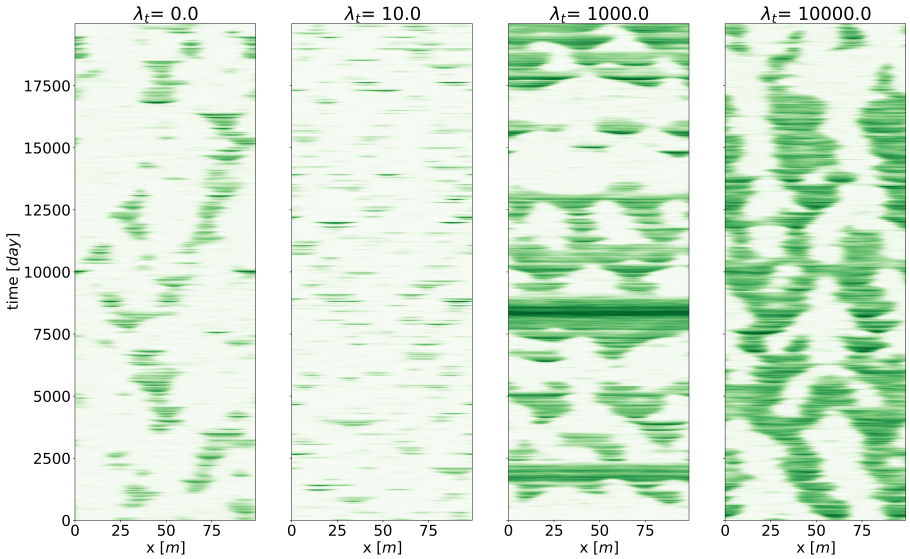


Figure 3.6: *Four realizations of the stochastic Rietkerk model with $\lambda_s = 1m$. The biomass is the variable shown. Each panel shows a representative realization with different temporal autocorrelations (λ_t). The temporal autocorrelation is defined as the correlation of a variable with itself as a function of time. The higher the temporal autocorrelation, the more the noise has memory and displays less abrupt variation. A illustration is shown in the Appendix of this chapter.*

us here is the one with one big pulse and one small pulse. Its existence spans from 0.6mmd^{-1} to less than 0.8mmd^{-1}. In the stochastic realization, the position of the second small pulse is not perfect because of noise. We clearly see that even if this mixed state with two pulses is not an equilibrium for this value of rainfall, it plays a role in the dynamics, hence the qualifier of "ghost" (Hastings et al. [2018a] and Morozov et al. [2020a]). Ghost attractors and unstable equilibria expand the resilience of the system because, in view of the orangutan in the forest, these configurations are new tree branches to cling to.

By demonstrating that resilience is bolstered by spatially heterogeneous noise and identifying critical timescales that influence biomass dynamics, we have provided valuable insights into the mechanisms underpinning ecological stability. Our findings emphasize the necessity of considering both stable and metastable states in resilience assessments, offering a more comprehensive understanding of ecosystem dynamics under varying perturbation regimes.

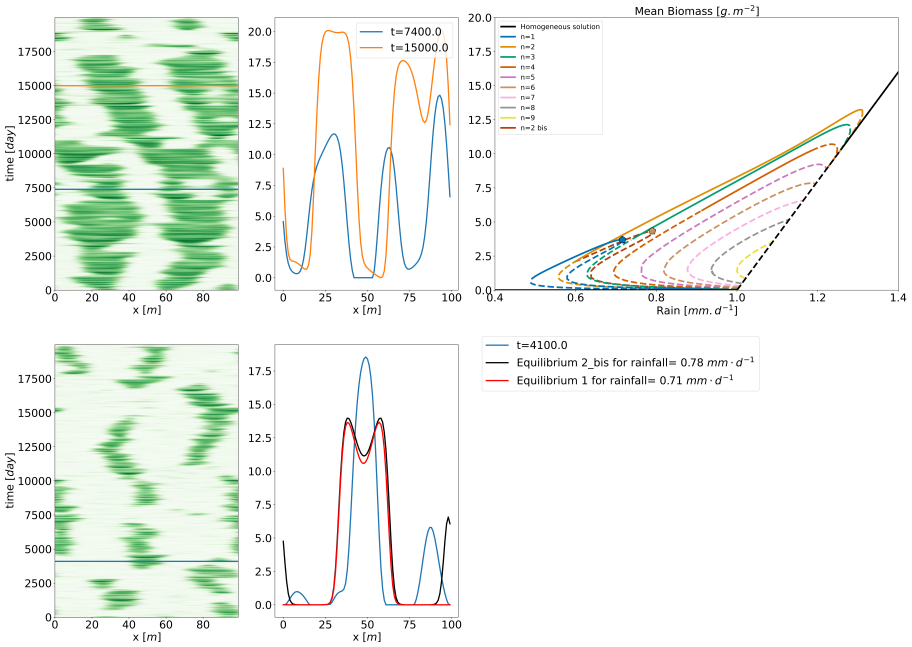


Figure 3.7: *Two realizations of the stochastic Rietkerk model with different noises. On the top-left panel, the parameters are* $R = 0.8 mm d^{-1}$, $\lambda_t = 1d$ *and* $\lambda_s = 10m$ *for the noise applied on the biomass, and* $\lambda_t = 10000d$ *and spatially homogeneous for the noise applied on the surface water. On the bottom-left panel, the parameters are* $R = 0.8 mm d^{-1}$, $\lambda_t = 1d$ *and* $\lambda_s = 15m$ *for the noise applied on the biomass, and* $\lambda_t = 1d$ *and spatially homogeneous for the noise applied on the surface water. The three horizontal lines mark the timing of the snapshots represented on the middle panels respectively. The top-right panel gives the bifurcation diagram with two pentagons marking the position of two equilibria shown on the bottom-center panel.*

3.5 Conclusions

The present study explored the effects of a spatially homogeneous perturbation, specifically a decrease in rainfall, on vegetation dynamics in a model system. By varying the rate of change in rainfall, we observed significant differences in the system's response. At slower rates, the system transitions through multiple stable states, including two and three pulse solutions. However, a critical rate of change at 10^{-3} mm.d^{-2} results in a direct shift from a homogeneous vegetated state to bare soil. This critical rate of change aligns with a critical timescale $\tau_{R_{\text{tip}}} \sim 1000$ d, much longer than the pulse destruction timescale $\tau_{\text{destruction}} = 52$d, highlighting

the dominance of slower processes in the system's behaviour under environmental changes.

3.5.1 Rearrangement timescale and system resilience

We identified a critical rearrangement timescale $\tau_{\text{rear}} \sim 1000\,\text{d}$, which corresponds to the system's response time to structural changes, such as the removal of a vegetation pulse. This timescale is pivotal for understanding the resilience and stability of vegetation patterns. By linking τ_{rear} to the diffusion coefficients of the system's components, we derived a scaling law that accurately predicts the rearrangement time, emphasizing the importance of spatial interactions in determining system dynamics.

3.5.2 Impact of spatial and temporal noise

We further investigated the resilience of the system under spatial and temporal noise, modeled as Gaussian stochastic processes. The experiments demonstrated that the spatial autocorrelation of noise significantly impacts pattern formation. Higher spatial correlations lead to reduced spatial variance and biomass, suggesting that more homogeneous noise disrupts more vegetation patterns. Temporal noise analysis revealed critical timescales—particularly around 10 days and 1000 days—corresponding respectively to the pulse and rearrangement timescales. These findings underscore the intricate balance between spatial and temporal scales in maintaining vegetation resilience.

3.5.3 Broader implications and multiple equilibria

Our analysis highlights the existence of multiple equilibria and the crucial role of slow timescales in spatially extended systems. The presence of ghost attractors and unstable equilibria broadens the system's resilience, offering additional configurations for the system to cling to, akin to tree branches in a forest. This multiplicity of stable and transient states enhances the system's capacity to adapt to gradual environmental changes, aligning with the concept of resilience as defined by Holling [1973].

In summary, this study contributes to clarify a complex interplay between rainfall perturbations, spatial and temporal noise, and vegetation dynamics. By identifying critical timescales and exploring the system's response to various perturbations, we provide valuable insights into the resilience and stability of vegetation systems. These findings contribute to a deeper understanding of ecological dynamics and the factors influencing the persistence of vegetation patterns under changing environmental conditions.

4

Modelling vegetation responses to rainfall intermittency using intermittent dynamical systems in semi-arid ecosystems

This chapter is based on the following paper in preparation:
Vanderveken, L. and Crucifix, M.: Modelling vegetation responses to rainfall intermittency using intermittent dynamical systems in semi-arid ecosystems.

Abstract

In semi-arid regions, vegetation patterns are highly sensitive to rainfall variability. This study investigates the use of intermittent dynamical systems to model local precipitation and its effects on vegetation biomass under two distinct water uptake functions. We demonstrate that intermittent rainfall dynamics offer a promising approach for capturing precipitation variability, even though our model does not incorporate seasonal cycles. Using simulators of intermittent precipitation to drive a vegetation model, we show that vegetation does not universally benefit from intermittent precipitation. Instead, the impact of precipitation varies with the type of intermittency applied and the water uptake function. Furthermore our results indicate that the intensity probability distribution of rainfall is a critical factor influencing biomass outcomes, with different intensity patterns producing distinct vegetation responses. This work represents the first study to drive vegetation patterns model with real intermittent dynamical systems, providing novel insights into the role of rainfall statistics in ecosystem dynamics. These findings lay a foundation for further research on rainfall variability and its ecological impacts, with implications for ecosystem management in water-limited environments.

4.1 Introduction

Arid and semi-arid environments have two main characteristics: water is the dominant controlling factor for biological processes, and precipitation is highly variable throughout the year occurring as infrequent and discrete events [Noy-Meir, 1973].

Water, as a controlling factor, forces the vegetation to adopt different strategies to cope with this scarcity [Meron, 2015]. One of these strategies is the formation of spatial patterns without external forcings (Murray [2003], Klausmeier [1999a]). The vegetation patterns allow vegetation to concentrate water in patches and create ecological niches through a process called "ecological engineering" [Gilad et al., 2007]. These patterns can be reproduced by reaction-diffusion models. In this context, the spatial patterns are caused by a combination of short-range facilitation and long-range inhibition (scale-dependent feedbacks [van de Koppel et al., 2005]). Four model classes are available differing by the physical processes that create the feedback and the variables involved in the dynamics (Gilad et al. [2007], Lejeune et al. [2004], Rietkerk et al. [2002a] and Klausmeier [1999a]). An extensive discussion on the different models can be found in Borgogno et al. [2009], Gandhi et al. [2019] and Siero [2020]. A well-known limitation of those models is that rainfall is supposed to be constant in time. Some studies explored the effect of a non-constant rainfall on vegetation patterns (Guttal and Jayaprakash [2007], Siteur et al. [2014a] Kletter et al. [2009], Eigentler and Sherratt [2020], Baudena et al. [2013], Rodriguez-Iturbe and Porporato [2005]). They modelled the intermittent precipitation variability in two ways: either with a seasonal input of a given quantity of water, or through a Poisson process.

Precipitation is a complex phenomenon. It implies processes on a wide range of scales, from the physics of micro droplets to the movement of air masses at synoptic scales [Trenberth et al., 2003]. This wide range creates temporal and spatial patterns in the water distribution around the world. Capturing these patterns with physical models, especially global models, remains a challenging task (Intergovernmental Panel on Climate Change (IPCC) [2023], Chagnaud et al. [2022]). Convective clouds, which are an important source of precipitation, involve much smaller spatial scales than the typical model resolution. Furthermore, in dry or semi-arid regions such as the Sahel, the precipitation regime is the product of a complex interplay of thermodynamic processes (e.g. convection) and dynamical processes (regional monsoon dynamics).

These complex dynamics tend to lead to intermittent behaviour at the global scale [Trenberth et al., 2017]. Specifically, in the Sahel, Nicholson et al. [2018] showed that precipitation in West Africa decomposes into a decadal mode, a seasonal cycle associated with the monsoon phenomenon, and, at a shorter time scale, intermittent behaviour. We use intermittency to qualify a process charac-

terised by period of inactivity with a random length (dry period) punctuated by shorts period of activity (precipitation due to storm for example).

To assess the effect of intermittency on vegetation dynamics at the spatial scale, it may be more suitable to use, rather than the output of a global model, small empirical models calibrated to reproduce the characteristics of observations. One possible approach would rely on fractal or multifractal iterative methods, referred to as cascades (Veneziano et al. [1996], Lovejoy [2018]). More simply, Kletter et al. [2009] and Baudena and Provenzale [2008] produce time series by modelling inter-arrival times between rainfall events as a stochastic variable from a Poisson distribution, known as point processes. However, Poisson processes do not capture the power-law distribution of inter-arrival times which characterises intermittent processes. Here, we aim to keep the simplicity of the Kletter et al. [2009] and Baudena and Provenzale [2008] approach, but yet, account for these power-law characteristics. In this context, the approach of Rigby and Porporato [2010] and Molini et al. [2009] provides an avenue. They explored dynamical systems known to produce intermittent time series with power-law distributions and identified the Pomeau-Manneville intermittency [Manneville and Pomeau, 1980] and On-Off intermittency [Platt et al., 1993] as good candidates to model precipitation. We will follow this strategy here, but with a focus on semi-arid areas. The first step of our analysis will thus be to identify suitable models to simulate precipitation in the Sahel.

Next, we will apply these models of intermittent precipitation to the Rietkerk vegetation patterns model [Rietkerk et al., 2002a], which we have previously analysed in Vanderveken and Crucifix [2024]. This model links the spatio-temporal distributions of biomass B with soil water W and surface water O as follows:

$$\begin{aligned}
\frac{\partial B}{\partial t} &= c g_{max} w u(W) B - dB + D_B \Delta B, \\
\frac{\partial W}{\partial t} &= \alpha O \frac{B + k_2 w_0}{B + k_2} - g_{max} w u(W) B - r_w W + D_W \Delta W, \\
\frac{\partial O}{\partial t} &= R - \alpha O \frac{B + k_2 w_0}{B + k_2} + D_O \Delta O,
\end{aligned} \tag{4.1}$$

where Δ is the Laplacian operator and R is the rainfall [mm.d^{-1}]. The rainfall is the external forcing of the system which we consider to be a spatially-independent function. The first term in the biomass equation represents water uptake by the plant. The first term in the soil water equation is linked to the infiltration rate of water in the soil that is enhanced by the presence of biomass. The factors in front of the Laplacians (ΔB, ΔW and ΔO) are the diffusion constants of the different quantities.

This model was used in previous work of ours [Vanderveken and Crucifix, 2024], but here we pay specific attention to the water uptake function $wu(W)$.

Indeed, different types of functional form of resource uptake have been identified (Holling [1966], Chesson et al. [2004]), and the way the plant uses the soil water is certainly critical for their survival in water-limited environment (Noy-Meir [1973], Chesson et al. [2004]). In the original model, the water uptake term is modelled with a so-called "type-II" functional form in the Holling classification also called Michaelis-Menten. The other function that we will consider is the type-III. It is characterized by an steep increase in water uptake for a certain value of soil water.

Type-II	Type-III
$wu(W) = \frac{W}{W+\phi_{II}}$	$wu(W) = \frac{W^4}{(W^4+\phi_{III})}$

Table 4.1: *Functional forms of the two types of water uptake considered in this study*

The parameters are the same as in Rietkerk et al. [2002a] for the type-II water uptake. The new parameters of type-III water uptake were chosen so that the bare soil equilibrium of the non-spatial model loses stability for the same value of constant rainfall. We chose to use the exponent-4 form of the type-III functional response to remain consistent with the previous work of Kletter et al. [2009] and Baudena and Provenzale [2008], both of whom refer to Chesson et al. [2004]. In that study, the authors examined the competition between two vegetation species across different environmental scenarios, depending on their resource uptake functions. Kletter et al. [2009] and Baudena and Provenzale [2008] have shown a positive effect of intermittent precipitation on vegetation for a type-III water uptake, but, again, they used a Poisson process as a model for intermittency. Hence, our work extends their contribution in two ways. On one hand, we consider truly intermittent precipitation forcing, based on an assessment of observations. Second, we discuss the effect of water uptake on the effect of intermittency. Our general objective is to contribute to the understanding of the mechanisms affecting vegetation resilience in semi-arid areas and determine the critical factors which condition this resilience.

4.2 Intermittent dynamical system as a model for precipitation.

An intermittent time series is characterized by extended periods of low activity, occasionally interrupted by bursts of activity. These prolonged low-activity phases are referred to as laminar times.

4.2.1 Models

Pomeau-Manneville intermittency was first observed in the Lorenz model [Manneville and Pomeau, 1979] as a transition to chaos. This transition occurs due to the destabilization of an equilibrium. Depending on the way in which the equilibrium loses its stability, three distinct types of Pomeau-Manneville intermittency can occur [Bergé et al., 1984]. Three possibilities arise depending on the behaviour of the Floquet multiplier. A Floquet multiplier is an eigenvalue that determines the stability of a periodic orbit in a dynamical system. If all multipliers lie inside the unit circle in the complex plane, the orbit is stable; otherwise, it is unstable. These types are distinguished by the nature of the laminar phases and how the system transitions to chaotic bursts.

The laminar phase in Pomeau-Manneville intermittency arises from the system's dynamics being slowed down near a marginally stable equilibrium, often referred to as a vanishing equilibrium. This behaviour is due to the presence of a channel in the phase space, which causes the system to linger near the equilibrium before transitioning to a burst. Several physical systems exhibit this type of intermittency, including Rayleigh-Bénard convection [Dubois et al., 1983], laser systems [Kingston et al., 2021], and electronic devices [Jeffries and Perez, 1982].

In this work, we focus on a specific form of Pomeau-Manneville intermittency known as type III intermittency (PM intermittency). This type occurs when the Floquet multiplier is real and crosses the unit circle at (-1). Type III intermittency can be described using the following map Pomeau and Manneville [1980]:

$$x_{n+1} = x_n + x_n^3 \ (\text{mod } 1), \tag{4.2}$$

where the laminar phase corresponds to the region where x_n is close to zero. The modulo operation serves as a reinjection mechanism, ensuring that the system remains within the bounded region and re-enters the laminar phase after escaping. Ignaccolo et al. [2001] introduced a continuous version of this map, described by the differential equation:

$$\dot{x} = x^3 + \rho_t, \tag{4.3}$$

where ρ_t represents a stochastic reinjection mechanism. Whenever $x = 1$, a random jump uniformly distributed in the interval $(-1, 0)$ is applied. The trajectory of the system thus consists of a series of events separated by laminar phases, where the length of the laminar phase follows a power-law distribution with an exponent of $-3/2$. The probability distribution of the variable x (intensity distribution) follows a power-law with an exponent of -2.

On-Off intermittency is based on a different mechanism for generating bursts in dynamical systems. This type of intermittency occurs due to the random or chaotic

destabilization of a stable attractor, as observed in several chaotic systems (Platt et al. [1993] Heagy et al. [1994]). The bursts in On-Off intermittency result from the stochastic destabilization of the system, leading to a sharp transition between the laminar and burst phases.

A simple model of On-Off intermittency can be described by the forced logistic map:

$$x_{n+1} = a y_n x_n (1 - x_n), \tag{4.4}$$

where y_n is a uniformly distributed random variable in the interval $[0, 1]$, and $a = 2.8$. Similar to Pomeau-Manneville intermittency, the distribution of laminar phase lengths follows a power-law with an exponent of $-3/2$, but in this case, the intensity distribution follows an exponent of -1.

4.2.2 Observations

We compare the distribution of laminar time and intensity from real-world precipitation data to those derived from theoretical models of intermittency. Specifically, we analyse data from various sources, including gauge, satellite, reanalysis, and Global Climate Models (GCM), as detailed in Table 4.2.

Type	Name	Period	Spatial resolution	Temporal resolution
Global climate model	EC-Earth33 [Döscher et al., 2022]	01/01/1970 - 31/12/2014	0.5°	Daily
Merged satellite/gauge data	GPCP [Huffman et al., 2001]	01/01/1997 - 31/12/2024	1°	Daily
Reanalysis	ERA5 [Hersbach et al., 2020]	01/01/1960 - 31/12/2023	0.25°	Daily
Merged gauge, satellite, and reanalysis data	MSWEP [Beck et al., 2017]	01/01/1979 - 31/12/2024	0.25°	3-hourly

Table 4.2: *Overview of the climate datasets*

An example of the time series from the MSWEP dataset, which provides 3-hourly precipitation data for the Sahel region, is shown in Fig. 4.1. This time series reveals a mixture of a seasonal and decadal forcing plus a random intermittent signal.

The laminar time distribution and intensity distribution across all datasets are shown in Fig. 4.2 and Fig. 4.3.

4.2.3 Results

We observe, accross all datasets (Fig. 4.2), that the distribution of laminar times follows a scaling law with an exponent of $-3/2$, consistent with both PM intermittency and On-Off intermittency. The only discrepancies appear in the ERA5 reanalysis and EC-Earth33 GCM datasets. The ERA5 data show an exponential probability distribution rather than a power-law, while the EC-Earth3 dataset exhibits a peak around one year. These discrepancies may be attributed to the

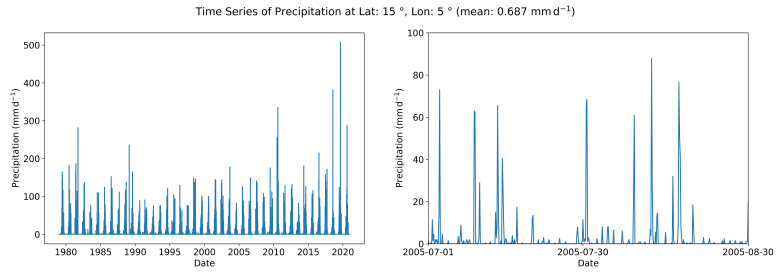


Figure 4.1: *Time series of precipitation in the Sahel region from the MSWEP dataset with a time resolution of 3 hours. The mean daily rainfall is* 0.68 *mm/d*

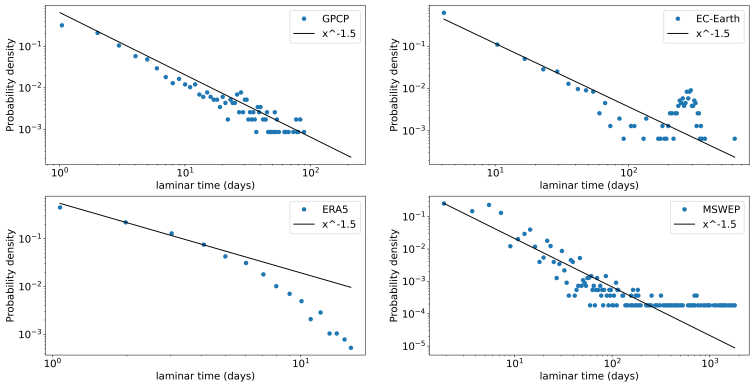


Figure 4.2: *Probability distribution of the laminar time in different datasets. The black line served as a visual aid identifying the power-law.*

limitations of the models in resolving strong convective systems, which are the primary drivers of precipitation in the Sahel region [Intergovernmental Panel on Climate Change (IPCC), 2023]. In the case of EC-Earth3, the pronounced peak likely corresponds to an overly strong seasonal cycle compared to observed data. The maximum laminar time observed across all datasets is one year, suggesting that the intermittent regime is valid across a wide range of timescales covered by the dataset, ranging from one day to one year. This contrasts with results for wetter climate: Rigby and Porporato [2010] found intermittency predominantly on sub-daily to daily timescales in wetter climates. We conclude that the laminar time distribution of Sahelian precipitation can be effectively modelled by PM intermittency or On-Off intermittency.

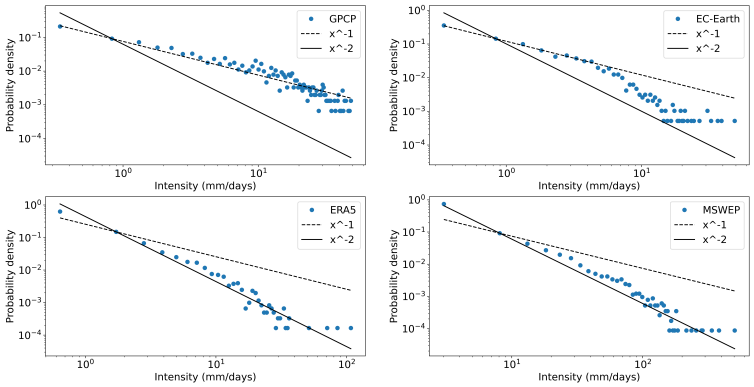


Figure 4.3: *Probability distribution of the intensity in different datasets. The black line served as a visual aid identifying the power-law.*

Regarding the intensity distribution (Fig. 4.3), the decision is not clear which one of On-Off intermittency or PM intermittency is the right model for precipitation. Indeed, the MSWEP and ERA5 show a power-law scaling with an exponent of -2. The EC-Earth3 and GPCP datasets follow a -1 scaling with an exponential decrease for the EC-Earth3 dataset. To explain this difference for EC-Earth3, we have to remember that the nature of precipitation in the Sahelian region is very convective. It is known that this particular type of events is difficult to represent in GCM like EC-Earth3 (Chagnaud et al. [2023], Intergovernmental Panel on Climate Change (IPCC) [2023]). This could explain the exponential decrease of the EC-Earth3 intensity distribution.

Consequently, we will use both PM and On-Off in the following to explore the effect of the two types of intermittency on vegetation patterns.

4.3 Effect of intermittent rainfall on vegetation patterns

We now examine the impact of intermittent forcing modelled by a intermittent dynamical system on vegetation patterns depending on the water uptake functional form. The two water uptake functional forms are shown in Fig. 4.4. From the graph of the two functions, one can see that type-II is advantaged compared to type-III for low value of soil water; but for high values of soil water type-III shows a higher water uptake. This difference is expected to play a role in the response of the system to the intermittent forcing.

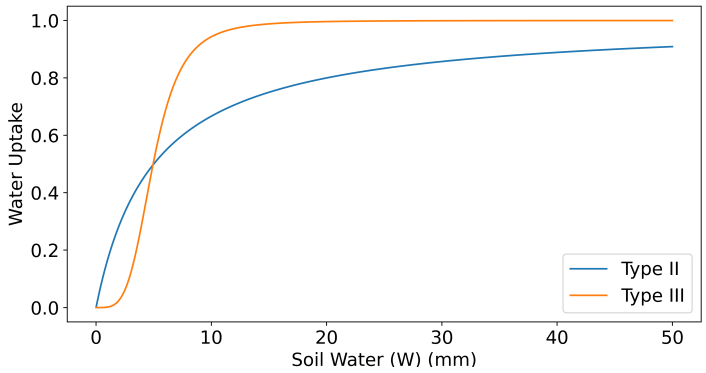


Figure 4.4: *Type-II and Type-III functional form of the water-uptake. For type-II, $\phi_{II} = 5mm$ and for type-III, $\phi_{III} = 600mm^4$.*

For each of the two water uptake functions, we ran the model with either constant, PM intermittency and On-Off intermittency, with specified rainfall rates ranging from 0 mm.d^{-1} to 1.5 mm.d^{-1}. Intermittent time series are obtained by scaling the output of the corresponding dynamical systems such that the mean rainfall meets the specification. The spatial domain is 2D-periodic with size $L = 200$ m.

With this setup, the vegetation disappears for the intermittent forcings. This, actually, was to be expected because without water allowing the vegetation to survive after a big water pulse the system goes to a desert state. As identified in Vanderveken and Crucifix [2024], the timing of disappearance of a vegetation bump is of the order of a dozen days. This implies that if the time separation between two rain events exceeds a few weeks, all the vegetation disappears. In nature, though, the vegetation in arid zone has adapted to this scenario with different strategies, typically by keeping biomass in seeds that can be activated by a rain pulse (Noy-Meir [1973], Schwinning and Sala [2004]). To take this strategy into account, we freeze the vegetation when the spatial mean of the biomass is lower than a given threshold. To achieve that, at each timestep, we compute the vegetation solution and calculate the spatial mean. If this quantity is smaller than 10^{-4} we replace this newly compute solution by the previous one.

The results for $L = 200$m are shown in Fig. 4.5.

From Fig. 4.5, we observe that the intermittency in rainfall further broadens the range of precipitation levels that vegetation can tolerate, potentially even more than incorporating a spatial component. We also see that PM intermittency consistently produces more biomass for the two water uptake functional forms. On the other hand, for the On-Off intermittency, the type-II water uptake produces

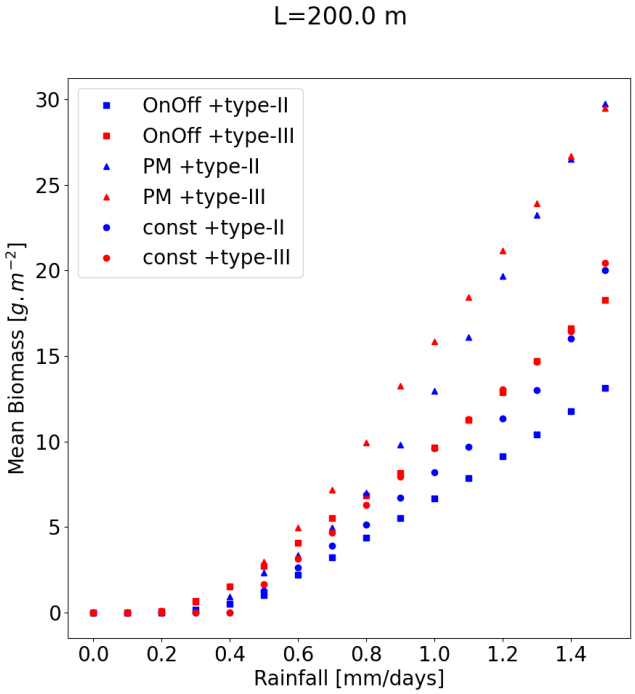


Figure 4.5: *Relation between the mean biomass and the mean rainfall. The blue marker represents the result with the type-II water uptake and the red markers the type-III water uptake. For each water uptake functional type, the model was integrated with a constant rainfall (round markers), a PM intermittency (square markers) and a On-Off intermittency (triangle markers). For each run, the Rietkerk model was integrated for 50 years.*

less mean biomass than the constant rainfall. For the type-III water uptake, we do not observe a change in the mean biomass compared to the constant rainfall. All these observations are summarized in Table 4.3.

	PM	On-Off
type-II water uptake	$\Uparrow$	$\Downarrow$
type-III water uptake	$\Uparrow$	$=$

Table 4.3: *Summary table of the effect of intermittent dynamical system and water uptake compared to a constant rainfall.*

4.3.1 Discussions

Previous research has highlighted the benefits of intermittency on vegetation growth under various water uptake models. For instance, Kletter et al. [2009] found that a type-III water uptake function outperformed both linear and type-II water uptake in supporting vegetation. However, our findings are more nuanced, by showing that outcomes vary depending on the type of intermittent forcing applied. This difference can be attributed to the distinct intensity distributions in each type of intermittency. Both On-Off and PM intermittencies follow a power-law distribution, but the On-Off intermittency has a gentler slope (exponent -1), while PM intermittency has a steeper slope (exponent -2). This distinction means that, for a given mean rainfall, PM intermittency exhibits higher rainfall maxima than On-Off intermittency.

These differences in rainfall intensity help explain why type-II water uptake underperforms with On-Off intermittency. Type-II water uptake is less efficient at low soil water levels, and because the rainfall maxima in On-Off intermittency are smaller than in PM, less vegetation can be sustained. However, with type-III water uptake, On-Off intermittency can generate mean biomass similar to that of constant rainfall, as the rainfall maxima are sufficient to activate the threshold effect in type-III uptake.

Overall, PM intermittency proves beneficial for both water uptake models, highlighting the significant role that intensity distribution plays.

4.4 Conclusions

The objective of this study was twofold: to assess the possibility to model intermittent precipitation in semi-arid regions with intermittent dynamical systems, and to study the impact of such an intermittent forcing on a vegetation patterns model.

First, we identified that Pomeau-Manneville type III and On-Off intermittency are both valid models for local precipitation by looking at two important features of rainfall for vegetation: dry spell length distribution and intensity distribution. In four different datasets, we observed a power-law in the dry period length and in intensity of the rainfall compatible with intermittent dynamical systems. A next development would be to improve the empirical model to take the seasonal cycle into account.

Next, we applied the two classes of intermittency to a vegetation patterns model with two different functional forms of water-uptake. We found that vegetation does not always benefit from intermittent precipitation. With a Pomeau-Manneville intermittency and both type-II and type-III water uptake, the model shows an increase in the mean biomass. With On-Off intermittency the type-II water uptake vegetation suffers from an intermittent forcing compared to a constant one. The

type-III water uptake vegetation showed no difference between the On-Off and the constant precipitation.

We argue that those distinctions are due to the difference in intensity distribution between the PM and On-Off intermittencies. These findings suggest that, depending on the water uptake model in use, intermittent rainfall does not always enhance mean biomass production—highlighting the nuanced relationship between rainfall patterns, water uptake models, and vegetation productivity. To further pursue this research, it is important to take into account rainwater partitioning which could significantly affect vegetation response, particularly in the presence of large rainfall pulses. Research by Siteur et al. [2014a] highlights that rainwater partitioning is crucial in such cases, as it influences water availability for vegetation and soil storage. Discussion on the validity of the functional forms would also be a welcome addition regarding the root system soil interaction (Javaux et al. [2013], Dubbert et al. [2023]).

Although past studies have explored the link between intermittency and vegetation patterns, this research is the first to use intermittent dynamical systems as the driver for rainfall variability. By providing an empirical basis for understanding how rainfall statistics impact vegetation response, this study advances the field of ecosystem modelling and lays the groundwork for future research on rainfall-vegetation interactions - in particular how vegetation-precipitation feedback could affect the intermittent behaviour of rainfall.

5

Conclusions and perspectives

Semi-arid regions, characterized by limited rainfall and poor soil conditions, cover approximately 15.2% of the global land surface [Scholes, 2020]. These areas are home to a significant portion of the world's population, with estimates ranging from 700 million to 1.2 billion people, and face numerous challenges, including high rainfall variability, increasing temperatures, and rising evaporative demand [Oki and Quiocho, 2020]. Land degradation and desertification are major concerns. To cope with water scarcity, vegetation organizes itself in patterns visible from the sky [Deblauwe et al., 2008]. The vegetation patterning is a strategy for vegetation to survive in a water limited environment through ecosystem engineering [Gilad et al., 2004]. With climate change intensifying, understanding the resilience of vegetation patterns is critical to predict how ecosystems will respond to shifting environmental conditions and associated stressors. To understand the creation of vegetation patterns, a number of models have been proposed in the litterature. Most of them are based on a scale-dependent feedback [Tietjen and Jeltsch, 2007]. In this thesis, we interested ourselves in the resilience of vegetation patterns and used the Rietkerk model [Rietkerk et al., 2002b]. This overarching topic was broken down into three sub-questions.

5.1 What are the possible intermediate states existing between a full vegetated state and bare soil and what is their influence on the dynamics?

In the first study, we used a linear stability analysis to compute the Turing zone of the homogeneous vegetated equilibrium in Rietkerk model. This analysis allowed

us to identify zero modes at the edge of the Turing zone. Zero modes correspond to marginally non-growing inhomogeneous solutions of the linearized equations. Their existence usually signals the presence of an instability that can send the system towards an inhomogeneous time-invariant solution in the full nonlinear model. We then used the zero modes at the edge of this Turing zone as starting points of spatially heterogeneous equilibrium branches. A continuation method was then used to compute the whole branches by changing the precipitation. The stability of the equilibria along the branches was evaluated by computing the eigenvalues of the Jacobian matrix. This construction allowed us to systematically identify multiple solutions, which appear in the form of different spatial configurations. Each of them is associated with a distinct number of vegetation bumps. We called those branches the main branches and they are recognizable by the fact that all vegetation pulses have the same heights.

The zero modes at the edge of the Turing zone were not the only ones identified. A number of zero modes appeared along the main branches and some of them were found at the transition between the stable and unstable parts of the main branches. We used the same continuation method as for tracing the main branches, and by starting from these bifurcation points we traced a new type of branches. Those branches are unstable for every values of rainfall, and appeared as a mixture of modes. We called "mixed states" the states found along these branches. We showed that mixed states are common and we conjectured that every zero mode along the main branches and even the mixed state branches should act as starting point for another branch of mixed states.

The mixed states do impact the dynamics of the system even though they are unstable. The existence of those vegetated state around which the system can spend some time effectively increases the resilience of the whole system. By considering a larger spatial domain, we showed that new branches appear and even that the range of precipitation that maintains vegetation has increased. This densification of equilibria, either by the existence of mixed states, or by the increased spatial domain size, enhances the resilience of the vegetation

5.2 How does the temporal and spatial structure of the perturbation affect the resilience of vegetation?

In the second study, we assessed how different types of perturbation affect the resilience of the vegetation. To this end, we first used a spatially homogeneous perturbation in the form of a linear decrease of rainfall with different rates. We observed significantly different responses of the system depending on the rate of change. At slower rates, the system goes through different spatial configurations. We identified a critical rate of change ($\tau_{R_{tip}}$) for which the system goes directly

from a homogeneous vegetated state to bare soil (R-tipping). This timescale was much larger than the one of destruction of a vegetation pulse. This highlights the importance of the slower timescale when considering the possibility of R-tipping.

Then, we identified two timescales by conducting a scale analysis of the model parameters: $\tau_{destruction}$ and τ_{rear}. The former is linked to the destruction of a vegetation pulse and is much shorter than the latter τ_{rear}. τ_{rear} — the rearrangement timescale — is linked to the movement of the vegetation pulses toward a stable spatial configuration. We demonstrated that, at this timescale, the ratio between the diffusion coefficients of the fast component (surface water) and the slow components (soil water and biomass) governs the dynamics. This highlighted the significance of the spatial component when examining the various timescales of the model.

The resilience of the system was also assessed against stochastic perturbations in the form of structured noise. The spatio-temporal structure of the noise was characterized by a temporal and spatial scale. We tested different noise configurations to evaluate which one destroyed vegetation most effectively. Four key insights emerged from this analysis. First, the higher the spatial autocorrelation of the noise, the greater the extent of vegetation mortality. Second, the vegetation mortality is at its highest when the temporal autocorrelation of the noise is close to the timescale of destruction of pulse ($\tau_{destruction}$). Third, the vegetation mortality is lower when the temporal autocorrelation is larger than the rearrangement time. Finally, the mixed state (highlighted in the previous study) appears to play a role even within the stochastic dynamics as the system spends some time around them. These findings suggest three things. First, the spatio-temporal structure of the perturbation is critical to evaluate the resilience. Second, knowledge of the internal timescale of the model could inform us about its sensitivity to different kinds of stochastic perturbations. Finally, the greater the density of equilibria within the potential landscape, the more resilient the system.

5.3 What is the impact of intermittent rainfall on vegetation resilience?

In the third study, we used the same model but in a 2D spatial configuration to study the effect of intermittency. This study was divided in two parts. First, we demonstrated that intermittent dynamical systems are good candidates to model the local precipitation in the Sahelian region. Indeed, the intermittent dynamical systems are characterized by a power-law distributions in two probability distribution: the waiting time between two bursting events and the intensity. We computed those two probability distribution for data sets from different origins: reanalysis, Earth System Model, Gauge product and satellite data. Our results showed that

two intermittent dynamical systems were compatible with the observations: the Pomeau-Manneville intermittency and the On-Off intermittency. Next, we investigated not only the effect of an intermittent precipitation but also the functional form of the water uptake. We considered two functional forms (type-II and type-III). The type-II is the one of the original Rietkerk model and the type-III is characterized by a strong threshold effect.

Our findings revealed that vegetation does not consistently benefit from intermittent precipitation. Under Pomeau-Manneville (PM) intermittency, the model indicated an increase in mean biomass for both type-II and type-III water uptake mechanisms. However, under On-Off intermittency, vegetation with type-II water uptake exhibits reduced performance compared to constant precipitation, while vegetation with type-III water uptake shows no discernible difference between the two precipitation regimes.

We attributed these differences to the distinct intensity distributions characteristic of PM and On-Off intermittencies. These results highlight that intermittent rainfall does not universally enhance mean biomass production; its impact depends on the specific water uptake model used. This underscores the complex interplay between rainfall patterns, water uptake mechanisms, and their impact on the resilience of vegetation.

5.4 General conclusions

This work explored the dynamics of vegetation resilience under varying environmental conditions, with a particular focus on intermediate states between fully vegetated and bare soil systems, the impact of perturbations on vegetation, and the effects of intermittent rainfall. The studies presented in this thesis contribute to a deeper understanding of the mechanisms that govern vegetation dynamics, particularly in response to spatial and temporal variations in precipitation.

The first study revealed that intermediate states between fully vegetated and bare soil landscapes play a crucial role in the resilience of vegetation. By identifying multiple stable spatial configurations, including mixed states, and examining how these states influence system dynamics, we demonstrated that the presence of such states can enhance system resilience. In particular, we showed that unstable equilibria, such as mixed states, can play a significant role in the dynamics, even though they are unstable, by increasing system resilience through their transient expression. Moreover, we showed that increasing domain size and the densification of equilibrium branches extend the range of precipitation that sustains vegetation, further strengthening the system's resilience.

The second study highlighted the importance of the spatial and temporal structure of perturbations in determining vegetation resilience. We found that both the rate of rainfall change and the autocorrelation of spatial and temporal noise

play significant roles in vegetation mortality. The study also revealed that internal timescales of the system, such as the creation and destruction of vegetation pulses, should be considered when assessing the system's sensitivity to perturbations. Our results emphasize that the denser the equilibrium landscape, the more resilient the system is to external disturbances.

In the third study, the focus shifted to the effects of intermittent rainfall on vegetation resilience. Through the investigation of intermittent rainfall patterns, we found that vegetation does not always benefit from such conditions. While Pomeau-Manneville intermittency was found to enhance biomass production in both type-II and type-III water uptake models, On-Off intermittency showed varying results. These differences were attributed to the distinct intensity distributions of the intermittent regimes. This study underscores the complexity of the relationship between rainfall patterns, water uptake mechanisms, and vegetation resilience, suggesting that intermittent rainfall does not universally lead to improved vegetation productivity.

Overall, this thesis emphasizes the critical role of spatial and temporal dynamics in shaping the resilience of vegetation to both deterministic and stochastic perturbations. The findings contribute to the growing body of knowledge on ecosystem resilience and provide insights that may inform future modelling efforts aimed at understanding and managing vegetation systems, especially in regions with variable rainfall patterns.

5.5 Scope, Limitations, and Future Perspectives

This section discusses the scope and generality of the results obtained in this thesis, addressing their applicability to other models and conditions, as well as potential research directions to build upon these findings.

5.5.1 Scope and Generality of Mixed States

The existence of mixed states was demonstrated within a specific subclass of vegetation pattern models. However, their presence in other models governed by scale-dependent feedback remains an open question. Since other models with scale-dependent feedback rely on the same fundamental mathematical mechanisms to generate stable regular patterns, it is plausible that similar mixed states, particularly in the form of unstable equilibria, could also exist in these models. Nevertheless, further investigations are required to confirm their presence and characterize their properties.

For phase-separation models, which also belong to the class of reaction-diffusion systems, the existence of mixed states is less clear. Unlike the structured, periodic

patterns seen in scale-dependent feedback models, phase-separation models often produce irregular spatial distributions, which may not support the formation of mixed states in the same manner. The precise conditions under which such states could emerge in these models remain to be explored.

Another factor that could influence the existence of mixed states is the role of boundary conditions. Whether mixed states are robust to different spatial constraints or require specific conditions for their formation is not yet fully understood. Addressing this question could provide deeper insight into the generality of these states across different ecological and physical systems.

Furthermore, the potential for mixed states to exist in spatially heterogeneous models raises intriguing questions. In such models, Bastiaansen et al. [2022] identified stable coexistence states, where distinct ecological phases occupy different regions of the spatial domain, separated by a well-defined interface. These coexistence states share conceptual similarities with mixed states in that they both reflect the capacity of spatial systems to sustain multiple configurations simultaneously. However, important distinctions exist. Coexistence states involve spatially separated phases that persist over time, while mixed states emerge as unstable modulations of equilibrium branches. Additionally, coexistence states can limit the impact of tipping events by confining transitions to specific regions, whereas mixed states influence system dynamics by altering the speed and pathway of transitions. Understanding the interplay between these two types of states in spatially heterogeneous models is an important direction for future research.

5.5.2 Resilience to Spatiotemporal Noise

A key aspect of this work was the study of vegetation resilience under structured noise. One limitation is that the analysis primarily focused on additive noise applied to the biomass. Recent studies, such as Hamster et al. [2024] on the Klausmeier model, have examined the effects of multiplicative noise on vegetation dynamics. Interestingly, their findings reveal a similar phenomenon to what was observed in this thesis: noise-induced transitions between spatial configurations. However, in our case, the use of additive noise also led to the creation of new vegetation pulses, an effect not observed under purely multiplicative noise.

A natural extension of this work would be to investigate combined noise effects, incorporating both the additive noise applied to surface water in this study and a multiplicative noise term affecting biomass dynamics. Additionally, analyzing the impact of noise on soil water dynamics could provide further insights. Given the role of soil moisture in modulating vegetation patterns, one may expect similar qualitative behaviors to those observed here, but with potentially distinct timescales and transition mechanisms.

5.5.3 Intermittent rainfall and vegetation pattterns

In the last chapter, we explore the effects of intermittent precipitation on vegetation patterns, but some limitations remain. First, the hypothesis that intermittent rainfall influences ecosystem stability needs to be tested with more real-world data to assess its validity. Additionally, our model does not account for seasonal variations in rainfall, which could significantly impact vegetation dynamics and should be considered in future work. Finally, while we use the Rietkerk model to study pattern formation, it may not be the most suitable framework for analyzing abrupt disturbances. A flow-kick model, as proposed by Gandhi et al. [2023], could be better suited for capturing the effects of sudden perturbations and warrants further investigation.

5.5.4 Future Perspectives

This thesis has explored how vegetation pattern resilience is influenced by internal system structure and external perturbations. In summary, we suggest the following perspectives.

Extending bifurcation analysis to more complex systems is a promising direction, as the identification of mixed states in vegetation models suggests that similar states could exist in other ecological systems. Investigating their presence in models that incorporate alternative feedbacks, nutrient cycling, or water transport mechanisms could reveal broader principles governing pattern formation and stability. Additionally, exploring other stochastic perturbations could further enrich our understanding of ecosystem stability under variable environmental conditions. While this work examined the effects of spatial and temporal noise, considering additional types of stochastic forcing, such as multiplicative noise or colored noise, may provide deeper insights.

Empirical validation of intermittent rainfall models is another crucial step. The hypothesis that intermittent dynamical systems effectively capture local precipitation variability should be tested against a broader set of field data. Comparing model predictions with high-resolution precipitation and vegetation measurements would strengthen confidence in their applicability. Moreover, incorporating plant community dynamics could enrich timescale interactions, as moving beyond single-species vegetation models to include multiple plant types with distinct growth rates, water uptake strategies, and resilience mechanisms would introduce additional timescales, offering a more comprehensive view of ecosystem responses to environmental variability.

Coupling vegetation and precipitation dynamics presents an exciting research avenue, as understanding how vegetation patterns influence precipitation intermittency, and vice versa, could provide new insights into feedbacks in eco-hydrological

systems. Finally, enhancing water uptake and soil models by refining the representation of plant-water interactions through small-scale models of root growth dynamics and water transport (e.g., Javaux et al. [2013]; Dubbert et al. [2023]) could improve the realism and predictive capability of large-scale vegetation models.

Among these perspectives, three directions stand out as particularly promising. First, improving water uptake and soil models is crucial for enhancing the realism of vegetation pattern simulations. By incorporating detailed plant-soil interactions, such as root dynamics and moisture transport, models can better capture key processes driving ecosystem resilience. Second, integrating plant community dynamics into vegetation models will provide a richer understanding of how biodiversity influences pattern formation, stability, and ecological function. Finally, coupling vegetation and precipitation dynamics represents a key step toward a holistic view of eco-hydrological feedbacks, shedding light on the interplay between ecosystem structure and climatic variability.

Exploring these directions can help expand on this thesis's findings and improve our understanding of vegetation resilience, pattern formation, and ecosystem dynamics in changing environments.

A

Supplement to Chapter 2

A.1 Numerical method

A.1.1 Time integration

The Rietkerk model consists of three reaction-diffusion equations. In order to integrate this system of equation in time, we use in this thesis a pseudo-spectral method. The system of equation is composed of a linear and an nonlinear part.

$$\begin{aligned} \frac{\partial B}{\partial t} &= f_B(B,W,O) + D_B \Delta B \\ \frac{\partial W}{\partial t} &= f_W(B,W,O) + D_W \Delta W \\ \frac{\partial O}{\partial t} &= f_O(B,W,O) + D_W \Delta W \end{aligned} \tag{A.1}$$

where $f_B(B,W,O)$, $f_W(B,W,O)$ and $f_O(B,W,O)$ are nonlinear terms and $D_B \Delta B$, $D_W \Delta W$, $D_O \Delta O$ are the diffusion terms and thus linear terms. This system of equation on a periodic domain of size $L = 100$ m can be simulated with a split-step Fourier spectral method. The idea is to solve the linear part in the spectral domain and the nonlinear part in the physical domain. For the linear part, we compute the Fast Fourier Transform to go to the spectral domain and use an backward Euler method to update the linear part. We then apply an inverse Fast Fourier Transform to obtain this partial update in physical space and apply a Forward Euler method to advance the nonlinear part. The spatial discretization is done with a spatial resolution of $dx = 1$ meter and the time step is $dt = 0.1$ days. The same integration scheme and discretization is used for the whole thesis.

A.1.2 Jacobian matrix

To apply the Newton-Raphson algorithm for the continuation method, we need to compute the Jacobian matrix of the system. Let's define N the number of spatial

discretization points. The vector of solution is then of size $3N$. To facilitate the definition of the second order differantiation matrix D_2 we rescale the spatial dimension from $L = 100$ m to 2π. The Jacobian matrix is then given by the following $3N \times 3N$ block matrix.

$$\mathcal{J} = \begin{bmatrix} \text{diag}(\partial F_B/\partial B) + D_P \frac{(2\pi)^2}{L^2} D_2 & \text{diag}(\partial F_B/\partial W) & \text{diag}(\partial F_B/\partial O) \\ \text{diag}(\partial F_W/\partial B) & \text{diag}(\partial F_W/\partial W) + D_W \frac{(2\pi)^2}{L^2} D_2 & \text{diag}(\partial F_W/\partial O) \\ \text{diag}(\partial F_O/\partial B) & \text{diag}(\partial F_O/\partial W) & \text{diag}(\partial F_O/\partial O) + D_O \frac{(2\pi)^2}{L^2} D_2 \end{bmatrix}$$

with

$$D_2 = \begin{pmatrix} \ddots & \vdots & \\ \ddots & -\frac{1}{2}\csc^2\left(\frac{2dx}{2}\right) & \\ \ddots & \frac{1}{2}\csc^2\left(\frac{dx}{2}\right) & \\ & -\frac{\pi^2}{3dx^2} - \frac{1}{6} & \\ & \frac{1}{2}\csc^2\left(\frac{dx}{2}\right) & \ddots \\ & -\frac{1}{2}\csc^2\left(\frac{2dx}{2}\right) & \\ & \vdots & \ddots \end{pmatrix}.$$

The Pyton implementation of those numerical schemes are available here `https://github.com/lvanderveken/Rietkerk_bif_diag`.

A.2 Random initial conditions with a fixed rainfall

Here, our goal is to verify that the stable pattern branches act as attractors in the dynamics of the system. To this end we specify a value of rainfall for which multiple stable equilibria exist. Starting with different initial conditions and evolving the system, we expect that different runs end in some of the different available stable states for the chosen rain value. To avoid favoring the attraction to a particular branch we opt for bare-soil initial conditions with random noise. Rainfall is set to $R = 1.1$ mm/d, for which the system has several stable equilibria (n = 2,3 and 4). The model is run for 5000 days with 500 distinct random initial conditions. Those are random from a uniform distribution (positive) noise on top of a homogeneous bare-soil equilibrium. Trajectories, projected onto a summary space (mean and maximum biomass) are shown in Fig. A.1. As this is a summary phase space - a projection of the full space - trajectories may appear to cross, but they do not in the full space. Out of the 500 runs, 465 land on the $n = 2$ equilibrium, and the others land on the $n = 3$ equilibrium. This indicates that the equilibria that we identify as stable are indeed those which attract trajectories. Having no trajectories on the $n = 4$ equilibrium suggests that the basin of attraction of the latter

is narrow and close to the homogeneous bare-soil equilibrium, with few chances for a trajectory starting from random initial conditions to be in the basin of attraction of that equilibrium or, in more informal terms, to evolve such as to pass close enough to the $n = 4$ equilibrium to land on it. The $n = 4$ equilibrium can however be reached with carefully designed initial conditions, such as a cosine with a wavenumber equal to $n\frac{2\pi}{L}$.

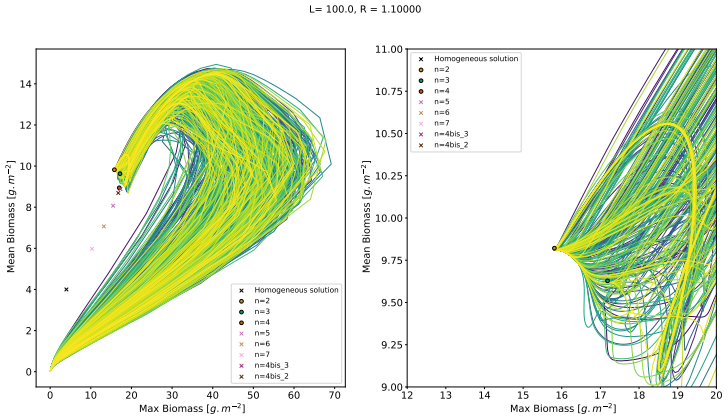


Figure A.1: *Trajectories on a summary phase space from random initial condition with a fixed rainfall $R = 1.1\,mm\,d^{-1}$. The relevant equilibria are shown. The stable equilibria are represented with a circle and the unstable equilibria with a cross.*

A.3 Identification of zero modes along branches

In section 2.2.3, we showed that a new type of equilibrium (mixed state) can appear at the transition between the unstable and the stable part of a branch. This transition is linked to the transition from positive to negative of the eigenvalue. For example at the transition on the $n = 4$ branch, we have three zero modes leading to the appearance of three mixed-state branches. In figure A.2, we propose a way to identify and represent those zero modes. Each of the panels is linked to one of the four highest eigenvalues. If this eigenvalue is positive the line is dashed, and if the eigenvalue is negative the line solid. With that in mind, let us focus on the $n = 4$ branch. We see that around $R = 0.91\,\mathrm{mm\,d}^{-1}$ the three first eigenvalues become negative. This means that there are three zero modes. We also observe that for the $n = 3$ branch, two eigenvalues switch from positive to negative around $R = 0.73\,\mathrm{mm\,d}^{-1}$. Again, this means that two mixed-state branches emanate from the zero mode at the transition.

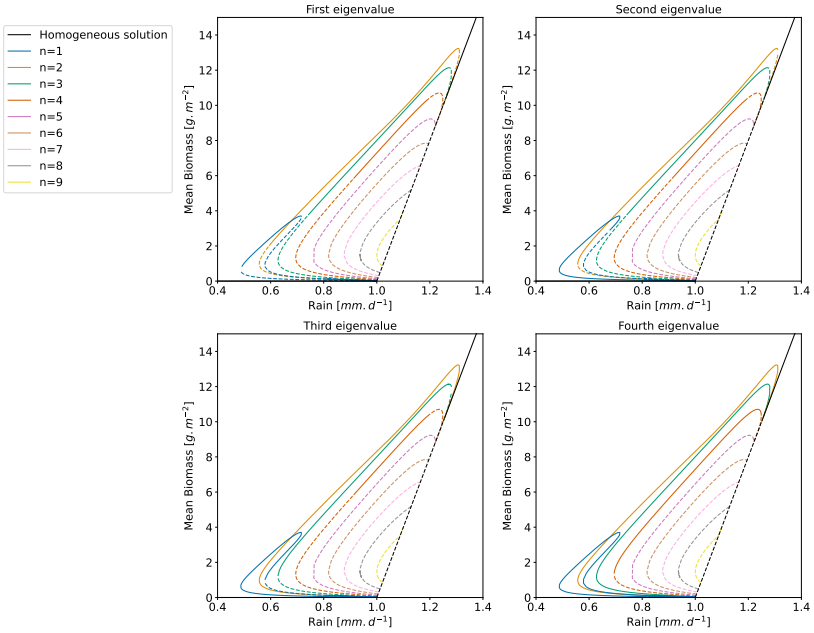


Figure A.2: *Bifurcation diagram for which the stability is computed based on the four highest eigenvalues. The solid line means that the eigenvalue considered is negative. The dashed line means that the eigenvalue is positive.*

B

Supplement to Chapter 3

B.1 Structured noise

The noise used in this paper is correlated both in time and space. We prescribe its standard deviation σ, length of spatial autocorrelation λ_s and time correlation λ_t with a period of L. To produce this noise, first, we computed the square root of the following covariance matrix where $N = 100$ is the number of spatial points.

$$\mathbf{A}_{i,j} = max\left(e^{\frac{-(x_i-x_j)^2}{\lambda_s^2}}, e^{\frac{-(L-|x_i-x_j|)^2}{\lambda_s^2}}\right)$$

Then we use an AR1 process in time to create the time dependence of the noise

$$x_{i,j} = x_{i,j} + (-c * x_{i,j}dt + \sqrt{dt}\sigma_e \sum_{k=1}^{n} \mathbf{A}_{j,k}\epsilon_k)$$

with $c = 1/\lambda_t$, dt the time step, $\sigma_e = \sigma\sqrt{2c}$ and ϵ_k a Gaussian random variable of zero mean and variance one.

The resulting noise is exemplified in B.1 and the temporal and spatial structure are shown in B.2.

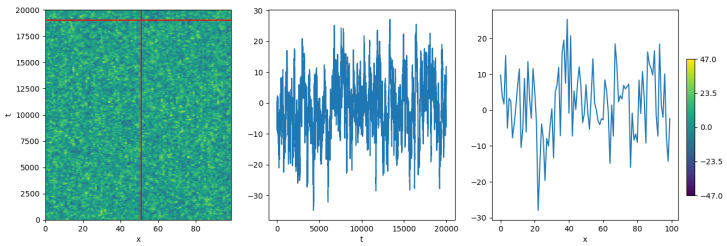


Figure B.1: *One realization of the structured noise with* $\sigma = 10$, $\lambda_t = 100$ *and* $\lambda_s = 1$. *On the left panel is shown the full noise. The vertical red line and the horizontal red line mark the position of the snapshots, those snapshots are represented on the middle panel for the vertical one, and on the right panel for the horizontal one.*

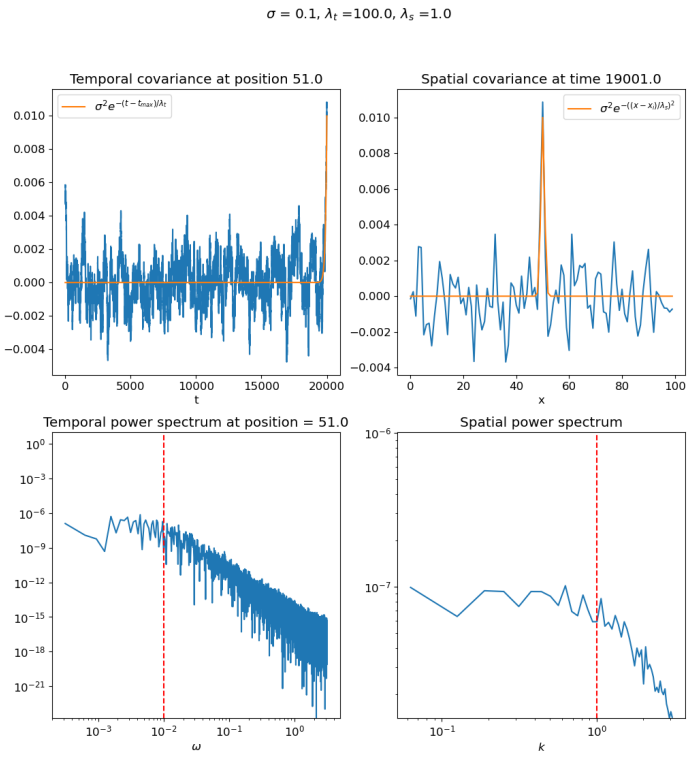


Figure B.2: *Mean over 50 realizations of the structured noise with* $\sigma = 10$, $\lambda_t = 100$ *and* $\lambda_s = 1$. *On the upper-left panel, the blue line is the mean over all the realizations with temporal autocorrelation at* $t = 20000$*; the orange line is the theoretical expectation. On the upper-right panel, the blue line is the mean over all the realizations of the spatial autocorrelation at* $x = 50$ *and the orange line is the theoretical expectation. On the bottom-left panel the blue line is the mean temporal power spectrum, and the vertical red dashed line is at* $1/\lambda_t$*.On the bottom-right panel the blue line is the mean spatial power spectrum and the vertical red dashed line is at* $1/\lambda_s$.

C

List of publications related to the thesis

First author

- Vanderveken, L., Martínez Montero, M. and Crucifix, M.: Existence and influence of mixed states in a model of vegetation patterns, *Nonlinear Processes in Geophysics*, **30(4)**, 585–599, https://doi.org/10.5194/npg-30-585-2023. (Chapter 2)
- Vanderveken, L. and Crucifix, M. (2025): Rate-Induced Transitions and Noise-Driven Resilience in Vegetation Pattern Dynamics, *Nonlinear Processes in Geophysics*, Accepted (Chapter 3)

Co-author

- Brovkin, V., Brook, E., Williams, J. W., Bathiany, S., Lenton, T. M., Barton, M., DeConto, R. M., Donges, J. F., Ganopolski, A., McManus, J., Praetorius, S., de Vernal, A., Abe-Ouchi, A., Cheng, H., Claussen, M., Crucifix, M., Gallopín, G., Iglesias, V., Kaufman, D. S., Kleinen, T., Lambert, F., van der Leeuw, S., Liddy, H., Loutre, M-F., McGee, D.,Rehfeld, K., Rhodes, R., Seddon, A. W. R., Trauth M. H., Vanderveken, L., Yu, Z. (2021). Past abrupt changes, tipping points and cascading impacts in the Earth system. *Nature Geoscience*, **14(8)**, 550–558. https://doi.org/10.1038/s41561-021-00790-5

References

Adams, B., Carr, J., Lenton, T. M., and White, A. (2003). One-dimensional daisyworld: Spatial interactions and pattern formation. *Journal of Theoretical Biology*, 223(4):505–513.

Alberti, T., Primavera, L., Vecchio, A., Lepreti, F., and Carbone, V. (2015). Spatial interactions in a modified Daisyworld model: Heat diffusivity and greenhouse effects. *Physical Review E - Statistical, Nonlinear, and Soft Matter Physics*, 92(5):1–11.

Ashwin, P., Wieczorek, S., Vitolo, R., and Cox, P. (2012). Tipping points in open systems: Bifurcation, noise-induced and rate-dependent examples in the climate system. *Philosophical Transactions of the Royal Society A: Mathematical, Physical and Engineering Sciences*, 370(1962):1166–1184.

Barbier, N., Couteron, P., Lejoly, J., Deblauwe, V., and Lejeune, O. (2006). Self-organized vegetation patterning as a fingerprint of climate and human impact on semi-arid ecosystems. *Journal of Ecology*, 94(3):537–547.

Bastiaansen, R., Dijkstra, H. A., and von der Heydt, A. S. (2022). Fragmented tipping in a spatially heterogeneous world. *Environmental Research Letters*, 17(4):045006.

Bastiaansen, R. and Doelman, A. (2019). The dynamics of disappearing pulses in a singularly perturbed reaction–diffusion system with parameters that vary in time and space. *Physica D: Nonlinear Phenomena*, 388:45–72.

Bastiaansen, R., Doelman, A., Eppinga, M. B., and Rietkerk, M. (2020). The effect of climate change on the resilience of ecosystems with adaptive spatial pattern formation. *Ecology Letters*, 23(3):414–429.

Bastiaansen, R., Jäibi, O., Deblauwe, V., Eppinga, M. B., Siteur, K., Siero, E., Mermoz, S., Bouvet, A., Doelman, A., and Rietkerk, M. (2018). Multistability of model and real dryland ecosystems through spatial self-organization. *Proceedings of the National Academy of Sciences of the United States of America*, 115(44):11256–11261.

Baudena, M. and Provenzale, A. (2008). Rainfall intermittency and vegetation feedbacks in drylands. *Hydrology and Earth System Sciences*, 12(2):679–689.

Baudena, M., von Hardenberg, J., and Provenzale, A. (2013). Vegetation patterns and soil–atmosphere water fluxes in drylands. *Advances in Water Resources*, 53:131–138.

Beck, H. E., Van Dijk, A. I., Levizzani, V., Schellekens, J., Miralles, D. G., Martens, B., and De Roo, A. (2017). MSWEP: 3-hourly 0.25° global gridded precipitation (1979-2015) by merging gauge, satellite, and reanalysis data. *Hydrology and Earth System Sciences*, 21(1):589–615.

Bel, G., Hagberg, A., and Meron, E. (2012). Gradual regime shifts in spatially extended ecosystems. *Theoretical Ecology*, 5(4):591–604.

Bergé, P., Pomeau, Y., and Vidal, C. (1984). *Order within chaos: towards a deterministic approach to turbulence*. Paris, wiley-inte edition.

Bernus, E., Marchal, J. Y., and Poncet, Y. (1993). The forgotten Sahel. *Revue tiers-monde*, 34.

Boers, N. (2021). Observation-based early-warning signals for a collapse of the Atlantic Meridional Overturning Circulation. *Nature Climate Change*, 11(8):680–688.

Borgogno, F., D'Odorico, P., Laio, F., and Ridolfi, L. (2009). Mathematical models of vegetation pattern formation in ecohydrology. *Reviews of Geophysics*, 41(1).

Brovkin, V., Claussen, M., Petoukhov, V., and Ganopolski, A. (1998). On the stability of the atmosphere-vegetation system in the Sahara/Sahel region. *Journal of Geophysical Research: Atmospheres*, 103(D24):31613–31624.

Buis, E., Veldkamp, A., Boeken, B., and van Breemen, N. (2009). Controls on plant functional surface cover types along a precipitation gradient in the Negev Desert of Israel. *Journal of Arid Environments*, 73(1):82–90.

Busse, F. H. (1978). Non-linear properties of thermal convection. *Reports on Progress in Physics*, 41(12):1929–1967.

Chagnaud, G., Panthou, G., Vischel, T., and Lebel, T. (2022). A synthetic view of rainfall intensification in the West African Sahel. *Environmental Research Letters*, 17(4).

Chagnaud, G., Panthou, G., Vischel, T., and Lebel, T. (2023). Capturing and Attributing the Rainfall Regime Intensification in the West African Sahel with CMIP6 Models. *Journal of Climate*, 36(6):1823–1843.

Charney, J. G. (1975). Dynamics of deserts and drought in the Sahel. *Quarterly Journal of the Royal Meteorological Society*, 101(428):193–202.

Chen, Y., Kolokolnikov, T., Tzou, J., and Gai, C. (2015). Patterned vegetation, tipping points, and the rate of climate change. *European Journal of Applied Mathematics*, 26(6):945–958.

Chesson, P., Gebauer, R. L., Schwinning, S., Huntly, N., Wiegand, K., Ernest, M. S., Sher, A., Novoplansky, A., and Weltzin, J. F. (2004). Resource pulses, species interactions, and diversity maintenance in arid and semi-arid environments. *Oecologia*, 141(2):236–253.

Claussen, M., Hoelzmann, P., Pachur, H.-J. J., Kubatzki, C., Brovkin, V., Ganopolski, A., Hoelzmann, P., and Pachur, H.-J. J. (1999). Simulation of an abrupt change in Saharan vegetation in the Mid-Holocene. *Geophysical Research Letters*, 26(14):2037–2040.

Conway, J. H. (1976). *On Numbers and Games*. Academic Press.

Dakos, V., Matthews, B., Hendry, A. P., Levine, J., Loeuille, N., Norberg, J., Nosil, P., Scheffer, M., and De Meester, L. (2019). Ecosystem tipping points in an evolving world. *Nature Ecology and Evolution*, 3(3):355–362.

Dakos, V., Scheffer, M., Van Nes, E. H., Brovkin, V., Petoukhov, V., and Held, H. (2008). Slowing down as an early warning signal for abrupt climate change. *Proceedings of the National Academy of Sciences of the United States of America*, 105(38):14308–14312.

Deblauwe, V., Barbier, N., Couteron, P., Lejeune, O., and Bogaert, J. (2008). The global biogeography of semi-arid periodic vegetation patterns. *Global Ecology and Biogeography*, 17(6):715–723.

Deblauwe, V., Couteron, P., Bogaert, J., and Barbier, N. (2012). Determinants and dynamics of banded vegetation pattern migration in arid climates. *Ecological Monographs*, 82(1):3–21.

Deblauwe, V., Couteron, P., Lejeune, O., Bogaert, J., and Barbier, N. (2011). Environmental modulation of self-organized periodic vegetation patterns in Sudan. *Ecography*, 34(6):990–1001.

Dekker, S. C., Rietkerk, M., and Bierkens, M. F. (2007). Coupling microscale vegetation-soil water and macroscale vegetation-precipitation feedbacks in semiarid ecosystems. *Global Change Biology*, 13(3):671–678.

DeMenocal, P., Ortiz, J., Guilderson, T., Adkins, J., Sarnthein, M., Baker, L., and Yarusinsky, M. (2000). Abrupt onset and termination of the African Humid Period:. *Quaternary Science Reviews*, 19(1-5):347–361.

Dijkstra, H. A. (2011). Vegetation pattern formation in a semi-arid climate. *International Journal of Bifurcation and Chaos*, 21(12):3497–3509.

D'Odorico, P., Laio, F., and Ridolfi, L. (2006). Vegetation patterns induced by random climate fluctuations. *Geophysical Research Letters*, 33(19):1–5.

Doelman, A., Rademacher, J. D., and Van Der Stelt, S. (2012). Hopf dances near the tips of busse balloons. *Discrete and Continuous Dynamical Systems - Series S*, 5(1):61–92.

Döscher, R., Acosta, M., Alessandri, A., Anthoni, P., Arsouze, T., Bergman, T., Bernardello, R., Boussetta, S., Caron, L.-P., Carver, G., Castrillo, M., Catalano, F., Cvijanovic, I., Davini, P., Dekker, E., Doblas-Reyes, F. J., Docquier, D., Echevarria, P., Fladrich, U., Fuentes-Franco, R., Gröger, M., v. Hardenberg, J., Hieronymus, J., Karami, M. P., Keskinen, J.-P., Koenigk, T., Makkonen, R., Massonnet, F., Ménégoz, M., Miller, P. A., Moreno-Chamarro, E., Nieradzik, L., van Noije, T., Nolan, P., O'Donnell, D., Ollinaho, P., van den Oord, G., Ortega, P., Prims, O. T., Ramos, A., Reerink, T., Rousset, C., Ruprich-Robert, Y., Le Sager, P., Schmith, T., Schrödner, R., Serva, F., Sicardi, V., Sloth Madsen, M., Smith, B., Tian, T., Tourigny, E., Uotila, P., Vancoppenolle, M., Wang, S., Wårlind, D., Willén, U., Wyser, K., Yang, S., Yepes-Arbós, X., and Zhang, Q. (2022). The EC-Earth3 Earth system model for the Coupled Model Intercomparison Project 6. *Geoscientific Model Development*, 15(7):2973–3020.

Dubbert, M., Couvreur, V., Kübert, A., and Werner, C. (2023). Plant water uptake modelling: added value of cross-disciplinary approaches. *Plant Biology*, 25(1):32–42.

Dubois, M., Rubio, M. A., and Berge, P. (1983). Experimental Evidence of Intermittencies Associated with a Subharmonic Bifurcation. *Physical Review Letters*, 51(25):2345–2345.

Dunkerley, D. L. and Brown, K. J. (2002). Oblique vegetation banding in the Australian arid zone: Implications for theories of pattern evolution and maintenance. *Journal of Arid Environments*, 51(2):163–181.

Eigentler, L. and Sherratt, J. A. (2019). Metastability as a Coexistence Mechanism in a Model for Dryland Vegetation Patterns. *Bulletin of Mathematical Biology*, 81(7):2290–2322.

Eigentler, L. and Sherratt, J. A. (2020). An integrodifference model for vegetation patterns in semi-arid environments with seasonality. *Journal of Mathematical Biology*, 81(3):875–904.

Fernandez-Oto, C., Escaff, D., and Cisternas, J. (2019). Spiral vegetation patterns in high-altitude wetlands. *Ecological Complexity*, 37(May 2018):38–46.

Feudel, U. (2023). Rate-induced tipping in ecosystems and climate: the role of unstable states, basin boundaries and transient dynamics. *Nonlinear Processes in Geophysics*, 30(4):481–502.

Gandhi, P., Iams, S., Bonetti, S., and Silber, M. (2019). Vegetation Pattern Formation in Drylands. In *Dryland Ecohydrology*, pages 469–509. Springer International Publishing, Cham.

Gandhi, P., Liu, L., and Silber, M. (2023). A Pulsed-Precipitation Model of Dryland Vegetation Pattern Formation. *SIAM Journal on Applied Dynamical Systems*, 22(2):657–693.

Gilad, E., Von Hardenberg, J., Provenzale, A., Shachak, M., and Meron, E. (2004). Ecosystem engineers: From pattern formation to habitat creation. *Physical Review Letters*, 93(9):98105.

Gilad, E., von Hardenberg, J., Provenzale, A., Shachak, M., and Meron, E. (2007). A mathematical model of plants as ecosystem engineers. *Journal of Theoretical Biology*, 244(4):680–691.

Govaerts, Y. and Lattanzio, A. (2007). Surface albedo response to sahel precipitation changes. *Eos, Transactions American Geophysical Union*, 88(3):25–26.

Gowda, K., Iams, S., and Silber, M. (2018). Signatures of human impact on self-organized vegetation in the Horn of Africa. *Scientific Reports*, 8(1):1–8.

Guttal, V. and Jayaprakash, C. (2007). Self-organization and productivity in semi-arid ecosystems: Implications of seasonality in rainfall. *Journal of Theoretical Biology*, 248(3):490–500.

Hamster, C., van Heijster, P., and Siero, E. (2024). Blurring the Busse balloon: Patterns in a stochastic Klausmeier model. pages 1–19.

Hastings, A., Abbott, K. C., Cuddington, K., Francis, T., Gellner, G., Lai, Y. C., Morozov, A., Petrovskii, S., Scranton, K., and Zeeman, M. L. (2018a). Transient phenomena in ecology. *Science*, 361(6406).

Hastings, A., Abbott, K. C., Cuddington, K., Francis, T., Gellner, G., Lai, Y. C., Morozov, A., Petrovskii, S., Scranton, K., and Zeeman, M. L. (2018b). Transient phenomena in ecology. *Science*, 361(6406).

Heagy, J. F., Platt, N., and Hammel, S. M. (1994). Characterization of on-off intermittency. *Physical Review E*, 49(2):1140–1150.

Hemming, C. F. (1965). Vegetation Arcs in Somaliland. *The Journal of Ecology*, 53(1):57.

Herman, R. J., Biasutti, M., and Kushnir, Y. (2023). Drivers of low-frequency Sahel precipitation variability: comparing CMIP5 and CMIP6 ensemble means with observations. *Climate Dynamics*, 61(9-10):4449–4470.

Hersbach, H., Bell, B., Berrisford, P., Hirahara, S., Horányi, A., Muñoz-Sabater, J., Nicolas, J., Peubey, C., Radu, R., Schepers, D., Simmons, A., Soci, C., Abdalla, S., Abellan, X., Balsamo, G., Bechtold, P., Biavati, G., Bidlot, J., Bonavita, M., De Chiara, G., Dahlgren, P., Dee, D., Diamantakis, M., Dragani, R., Flemming, J., Forbes, R., Fuentes, M., Geer, A., Haimberger, L., Healy, S., Hogan, R. J., Hólm, E., Janisková, M., Keeley, S., Laloyaux, P., Lopez, P., Lupu, C., Radnoti, G., de Rosnay, P., Rozum, I., Vamborg, F., Villaume, S., and Thépaut, J. (2020). The ERA5 global reanalysis. *Quarterly Journal of the Royal Meteorological Society*, 146(730):1999–2049.

HilleRisLambers, R., Rietkerk, M., Van Den Bosch, F., Prins, H. H., and De Kroon, H. (2001). Vegetation pattern formation in semi-arid grazing systems. *Ecology*, 82(1):50–61.

Holling, C. (1973). Resilience and Stability of Ecological Systems. *Annual Review of Ecology and Systematics*, 4:1–23.

Holling, C. S. (1966). The Functional Response of Invertebrate Predators to Prey Density. *Memoirs of the Entomological Society of Canada*, 98(S48):5–86.

Hopcroft, P. O. and Valdes, P. J. (2021). Paleoclimate-conditioning reveals a North Africa land–atmosphere tipping point. *Proceedings of the National Academy of Sciences*, 118(45):1–7.

Huffman, G. J., Adler, R. F., Morrissey, M. M., Bolvin, D. T., Curtis, S., Joyce, R., McGavock, B., and Susskind, J. (2001). Global Precipitation at One-Degree Daily Resolution from Multisatellite Observations. *Journal of Hydrometeorology*, 2(1):36–50.

Ignaccolo, M., Grigolini, P., and Rosa, A. (2001). Sporadic randomness: The transition from the stationary to the nonstationary condition. *Physical Review E - Statistical Physics, Plasmas, Fluids, and Related Interdisciplinary Topics*, 64(2):11.

Intergovernmental Panel on Climate Change (IPCC) (2023). Water Cycle Changes. In *Climate Change 2021 – The Physical Science Basis*, pages 1055–1210. Cambridge University Press.

Javaux, M., Couvreur, V., Vanderborght, J., and Vereecken, H. (2013). Root Water Uptake: From Three-Dimensional Biophysical Processes to Macroscopic Modeling Approaches. *Vadose Zone Journal*, 12(4):1–16.

Jeffries, C. and Perez, J. (1982). Observation of a Pomeau-Manneville intermittent route to chaos in a nonlinear oscillator. *Physical Review A*, 26(4):2117–2122.

Kéfi, S., Domínguez-García, V., Donohue, I., Fontaine, C., Thébault, E., and Dakos, V. (2019). Advancing our understanding of ecological stability. *Ecology Letters*, 22(9):1349–1356.

Kéfi, S., Rietkerk, M., Alados, C. L., Pueyo, Y., Papanastasis, V. P., ElAich, A., and De Ruiter, P. C. (2007). Spatial vegetation patterns and imminent desertification in Mediterranean arid ecosystems. *Nature*, 449(7159):213–217.

Kingston, S. L., Mishra, A., Balcerzak, M., Kapitaniak, T., and Dana, S. K. (2021). Instabilities in quasiperiodic motion lead to intermittent large-intensity events in Zeeman laser. *Physical Review E*, 104(3):034215.

Klausmeier, C. A. (1999a). Regular and Irregular Patterns in Semiarid Vegetation. *Science*, 284(5421):1826–1828.

Klausmeier, C. A. (1999b). Regular and irregular patterns in semiarid vegetation. *Science*, 284(5421):1826–1828.

Kletter, A. Y., von Hardenberg, J., Meron, E., and Provenzale, A. (2009). Patterned vegetation and rainfall intermittency. *Journal of Theoretical Biology*, 256(4):574–583.

Kröpelin, S., Verschuren, D., Lézine, A. M., Eggermont, H., Cocquyt, C., Francus, P., Cazet, J. P., Fagot, M., Rumes, B., Russell, J. M., Darius, F., Conley, D. J., Schuster, M., Von Suchodoletz, H., and Engstrom, D. R. (2008). Climate-driven ecosystem succession in the Sahara: The past 6000 years. *Science*, 320(5877):765–768.

Lefever, R. and Lejeune, O. (1997). On the origin of tiger bush. *Bulletin of Mathematical Biology*, 59(2):263–294.

Lejeune, O., Tlidi, M., and Lefever, R. (2004). Vegetation spots and stripes: Dissipative structures in arid landscapes. *International Journal of Quantum Chemistry*, 98(2):261–271.

Lenton, T. M., Held, H., Kriegler, E., Hall, J. W., Lucht, W., Rahmstorf, S., and Schellnhuber, H. J. (2008). Tipping elements in the Earth's climate system. *Proceedings of the National Academy of Sciences*, 105(6):1786–1793.

Liu, Q. X., Rietkerk, M., Herman, P. M., Piersma, T., Fryxell, J. M., and van de Koppel, J. (2016). Phase separation driven by density-dependent movement: A novel mechanism for ecological patterns. *Physics of Life Reviews*, 19(July):107–121.

Lovejoy, S. (2018). Spectra, intermittency, and extremes of weather, macroweather and climate. *Scientific Reports*, 8(1):1–13.

Macfadyen, W. A. (1950a). Soil and Vegetation in British Somaliland. *Nature*, 165(4186):121–121.

Macfadyen, W. A. (1950b). Vegetation Patterns in the Semi-Desert Plains of British Somaliland. *The Geographical Journal*, 116(4/6):199.

Manneville, P. and Pomeau, Y. (1979). Intermittency and the Lorenz model. *Physics Letters A*, 75(1-2):1–2.

Manneville, P. and Pomeau, Y. (1980). Different ways to turbulence in dissipative dynamical systems. *Physica D: Nonlinear Phenomena*, 1(2):219–226.

Meron, E. (2015). *Nonlinear physics of ecosystems*. CRC Press.

Molini, A., Katul, G. G., and Porporato, A. (2009). Revisiting rainfall clustering and intermittency across different climatic regimes. *Water Resources Research*, 45(11):1–13.

Moreno-De Las Heras, M., Saco, P. M., Willgoose, G. R., and Tongway, D. J. (2012). Variations in hydrological connectivity of Australian semiarid landscapes indicate abrupt changes in rainfall-use efficiency of vegetation. *Journal of Geophysical Research: Biogeosciences*, 117(3):1–15.

Morozov, A., Abbott, K., Cuddington, K., Francis, T., Gellner, G., Hastings, A., Lai, Y. C., Petrovskii, S., Scranton, K., and Zeeman, M. L. (2020a). Long transients in ecology: Theory and applications. *Physics of life reviews*, 32:1–40.

Morozov, A., Abbott, K., Cuddington, K., Francis, T., Gellner, G., Hastings, A., Lai, Y. C., Petrovskii, S., Scranton, K., and Zeeman, M. L. (2020b). Long transients in ecology: Theory and applications. *Physics of life reviews*, 32:1–40.

Mueller, J. (2013). Floristic and Structural Pattern and Current Distribution of Tiger Bush Vegetation in Burkina Faso (West Africa), Assessed By Means of Belt Transects and Spatial Analysis. *Applied Ecology and Environmental Research*, 11(2):153–171.

Murray, J. D. (2003). *Mathematical Biology II : Spatial Models and Biomedical Applications , Third Edition*. Springer.

Nicholson, S. E., Fink, A. H., and Funk, C. (2018). Assessing recovery and change in West Africa's rainfall regime from a 161-year record. *International Journal of Climatology*, 38(10):3770–3786.

Noy-Meir, I. (1973). Desert Ecosystems: Environment and Producers. *Annual Review of Ecology and Systematics*, 4(1):25–51.

Oki, T. and Quiocho, R. E. (2020). Economically challenged and water scarce: identification of global populations most vulnerable to water crises. *International Journal of Water Resources Development*, 36(2-3):416–428.

Pelletier, J. D., Delong, S. B., Orem, C. A., Becerra, P., Compton, K., Gressett, K., Lyons-Baral, J., McGuire, L. A., Molaro, J. L., and Spinler, J. C. (2012). How do vegetation bands form in dry lands? Insights from numerical modeling and field studies in southern Nevada, USA. *Journal of Geophysical Research: Earth Surface*, 117(4):1–18.

Penny, G. G., Daniels, K. E., and Thompson, S. E. (2013). Local properties of patterned vegetation: Quantifying endogenous and exogenous effects. *Philosophical Transactions of the Royal Society A: Mathematical, Physical and Engineering Sciences*, 371(2004).

Platt, N., Spiegel, E. A., and Tresser, C. (1993). On-off intermittency: A mechanism for bursting. *Physical Review Letters*, 70(3):279–282.

Pomeau, Y. and Manneville, P. (1980). Intermittent transition to turbulence in dissipative dynamical systems. *Communications in Mathematical Physics*, 74(2):189–197.

Rietkerk, M., Bastiaansen, R., Banerjee, S., van de Koppel, J., Baudena, M., and Doelman, A. (2021). Evasion of tipping in complex systems through spatial pattern formation. *Science*, 374(6564).

Rietkerk, M., Boerlijst, M. C., van Langevelde, F., HilleRisLambers, R., van de Koppel, J., Kumar, L., Prins, H. H. T., and de Roos, A. M. (2002a). Self-Organization of Vegetation in Arid Ecosystems. *The American Naturalist*, 160(4):524–530.

Rietkerk, M., Dekker, S. C., de Ruiter, P. C., and van de Koppel, J. (2004). Self-Organized Patchiness and Catastrophic Shifts in Ecosystems. *Science*, 305(5692):1926–1929.

Rietkerk, M. and van de Koppel, J. (2008a). Regular pattern formation in real ecosystems. *Trends in Ecology and Evolution*, 23(3):169–175.

Rietkerk, M. and van de Koppel, J. (2008b). Regular pattern formation in real ecosystems. *Trends in Ecology and Evolution*, 23(3):169–175.

Rietkerk, M., van de Koppel, J., Kumar, L., van Langevelde, F., and Prins, H. H. (2002b). The ecology of scale. *Ecological Modelling*, 149(1-2):1–4.

Rigby, J. R. and Porporato, A. (2010). Precipitation, dynamical intermittency, and sporadic randomness. *Advances in Water Resources*, 33(8):923–932.

Rodriguez-Iturbe, I. and Porporato, A. (2005). *Ecohydrology of water-controlled ecosystems: Soil moisture and plant dynamics*, volume 9780521819. Cambridge University Press.

Scheffer, M., Holmgren, M., Brovkin, V., and Claussen, M. (2005). Synergy between small- And large-scale feedbacks of vegetation on the water cycle. *Global Change Biology*, 11(7):1003–1012.

Schlesinger, W. H., Reynolds, J. F., Cunningham, G. L., Huenneke, L. F., Jarrell, W. M., Virginia, R. A., and Whitford, W. G. (1990). Biological Feedbacks in Global Desertification. *Science*, 247(4946):1043–1048.

Scholes, R. J. (2020). The future of semi-arid regions: A weak fabric unravels. *Climate*, 8(3):1–11.

Schwinning, S. and Sala, O. E. (2004). Hierarchy of responses to resource pulses in arid and semi-arid ecosystems. *Oecologia*, 141(2):211–220.

Sheffer, E., von Hardenberg, J., Yizhaq, H., Shachak, M., and Meron, E. (2013). Emerged or imposed: A theory on the role of physical templates and self-organisation for vegetation patchiness. *Ecology Letters*, 16(2):127–139.

Sherratt, J. A. (2013). History-dependent patterns of whole ecosystems. *Ecological Complexity*, 14:8–20.

Sherratt, J. A., Smith, M. J., and Rademacher, J. D. (2009). Locating the transition from periodic oscillations to spatiotemporal chaos in the wake of invasion. *Proceedings of the National Academy of Sciences of the United States of America*, 106(27):10890–10895.

Siero, E. (2020). Resolving soil and surface water flux as drivers of pattern formation in Turing models of dryland vegetation: A unified approach. *Physica D: Nonlinear Phenomena*, 414:132695.

Siero, E., Doelman, A., Eppinga, M. B., Rademacher, J. D. M., Rietkerk, M., and Siteur, K. (2015). Striped pattern selection by advective reaction-diffusion systems: Resilience of banded vegetation on slopes. *Chaos: An Interdisciplinary Journal of Nonlinear Science*, 25(3):1–17.

Sinclair, A. R. E. and Fryxell, J. M. (1985). The Sahel of Africa: ecology of a disaster. *Canadian Journal of Zoology*, 63(5):987–994.

Siteur, K., Eppinga, M. B., Karssenberg, D., Baudena, M., Bierkens, M. F., and Rietkerk, M. (2014a). How will increases in rainfall intensity affect semiarid ecosystems? *Water Resources Research*, 50(7):5980–6001.

Siteur, K., Liu, Q.-X., Rottschäfer, V., van der Heide, T., Rietkerk, M., Doelman, A., Boström, C., and van de Koppel, J. (2023). Phase-separation physics underlies new theory for the resilience of patchy ecosystems. *Proceedings of the National Academy of Sciences*, 120(2):2017.

Siteur, K., Siero, E., Eppinga, M. B., Rademacher, J. D., Doelman, A., and Rietkerk, M. (2014b). Beyond Turing: The response of patterned ecosystems to environmental change. *Ecological Complexity*.

Thiery, J. M., D'Herbes, J.-M., and Valentin, C. (1995). A Model Simulating the Genesis of Banded Vegetation Patterns in Niger. *The Journal of Ecology*, 83(3):497.

Tietjen, B. and Jeltsch, F. (2007). Semi-arid grazing systems and climate change: A survey of present modelling potential and future needs. *Journal of Applied Ecology*, 44(2):425–434.

Trenberth, K. E., Dai, A., Rasmussen, R. M., and Parsons, D. B. (2003). The changing character of precipitation. *Bulletin of the American Meteorological Society*, 84(9):1205–1217+1161.

Trenberth, K. E., Zhang, Y., and Gehne, M. (2017). Intermittency in precipitation: Duration, frequency, intensity, and amounts using hourly data. *Journal of Hydrometeorology*, 18(5):1393–1412.

Turing, A. M. (1952). The chemical basis of morphogenesis. *Philosophical Transactions of the Royal Society of London. Series B, Biological Sciences*, 237(641):37–72.

Valentin, C., D'Herbès, J. M., and Poesen, J. (1999). Soil and water components of banded vegetation patterns. *Catena*, 37(1-2):1–24.

Van De Koppel, J., Altieri, A. H., Silliman, B. R., Bruno, J. F., and Bertness, M. D. (2006). Scale-dependent interactions and community structure on cobble beaches. *Ecology Letters*, 9(1):45–50.

van de Koppel, J., Rietkerk, M., Dankers, N., and Herman, P. M. (2005). Scale-dependent feedback and regular spatial patterns in young mussel beds. *The American naturalist*, 165(3).

Van De Leemput, I. A., Van Nes, E. H., and Scheffer, M. (2015). Resilience of alternative states in spatially extended ecosystems. *PLoS ONE*, 10(2):1–17.

Van Der Stelt, S., Doelman, A., Hek, G., and Rademacher, J. D. (2013). Rise and fall of periodic patterns for a generalized klausmeier-gray-scott model. *Journal of Nonlinear Science*, 23(1):39–95.

Vanderveken, L. and Crucifix, M. (2024). Rate-Induced Transitions and Noise-Driven Resilience in Vegetation Pattern Dynamics. *in open discussion (NPG)*, (September).

Vanderveken, L., Martínez Montero, M., and Crucifix, M. (2023). Existence and influence of mixed states in a model of vegetation patterns. *Nonlinear Processes in Geophysics*, 30(4):585–599.

Veneziano, D., Bras, R. L., and Niemann, J. D. (1996). Nonlinearity and self-similarity of rainfall in time and a stochastic model. *Journal of Geophysical Research: Atmospheres*, 101(D21):26371–26392.

von Hardenberg, J., Meron, E., Shachak, M., and Zarmi, Y. (2001). Diversity of vegetation patterns and desertification. *Physical Review Letters*, 87(19):198101–1–198101–4.

Walker, B., Holling, C. S., Carpenter, S. R., and Kinzig, A. (2004). Resilience, adaptability and transformability in social-ecological systems. *Ecology and Society*, 9(2).

Walther, O. J. and Retaillé, D. (2021). Mapping the Sahelian Space. In *The Oxford Handbook of the African Sahel*, pages 15–34. Oxford University Press.

Zelnik, Y. R., Kinast, S., Yizhaq, H., Bel, G., and Meron, E. (2013). Regime shifts in models of dryland vegetation. *Philosophical Transactions of the Royal Society A: Mathematical, Physical and Engineering Sciences*, 371(2004).

Zelnik, Y. R. and Meron, E. (2018). Regime shifts by front dynamics. *Ecological Indicators*, 94(February):544–552.

Zelnik, Y. R., Meron, E., and Bel, G. (2016). Localized states qualitatively change the response of ecosystems to varying conditions and local disturbances. *Ecological Complexity*, 25:26–34.

Zelnik, Y. R., Uecker, H., Feudel, U., and Meron, E. (2017). Desertification by front propagation? *Journal of Theoretical Biology*, 418(November 2016):27–35.